PRECIPITATION BEHAVIOUR OF THE Cu-30% Ni-2% Nb-4% Fe ALLOY

by

Costas Kokkinoplitis
Department of Mechanical Engineering
Metallurgy

MASTER OF SCIENCE

Winnipeg, Manitoba

ISBN 0-315-33595-5

PRECIPITATION BEHAVIOUR OF THE

Cu-30% Ni-2% Nb-4% Fe ALLOY

by

Costas Kokkinoplitis

A thesis submitted to the Faculty of Graduate Studies of the University of Manitoba in partial fulfillment of the requirements of the degree of

MASTER OF SCIENCE

I hereby declare that I am the sole author of this publication.

I authorize the University of Manitoba to lend this publication to other institutions or individuals for the purpose of scholarly research.

Costas Kokkinoplitis

I further authorize the University of Manitoba to reproduce this publication by photocopying or by other means, in total or in part, at the request of other institutions or individuals for the purpose of scholarly research.

Costas Kokkinoplitis

The University of Manitoba requires the signatures of all persons using or photocopying this publication. Please sign below, and give address and date.

ACKNOWLEDGEMENTS

I wish to express my sincere thanks to Dr. M. C. Chaturvedi for his guidance and encouragement throughout the course of this work. I would also like to thank my colleagues and friends who have contributed towards the completion of this work. I want to take this opportunity to thank the technicians in the metallurgical sciences laboratory and in particular Mr. J. Van Dorp for their invaluable technical assistance.

The financial assistance from the University of Manitoba and Dr. M. C. Chaturvedi is gratefully acknowledged.

ABSTRACT

The precipitation process in a Cu-30Ni-2Nb-4Fe alloy was investigated on aging at 873 K [600°C] and 973 K [700°C) after water quenching from 1373 K [1100°C] using mechanical testing, x-ray diffraction, electron microscopy and EDS analysis.

On aging at 873 K the yield stress and the ultimate tensile stress increase monotonously with increasing aging time. The decomposition at this temperature occured through the fcc-γ'-$L1_2$ Ni_3Nb phase on the (100) matrix planes. No cellular precipitation or other transformation reaction was observed at this temperature.

However, the strengthening process at 973 K was accelerated dramatically. A peak yield strength increment of 380 MPa was attained in less than 10 hours of aging. The mode of precipitation at this temperature was of the discontinuous type:

γ(supersaturated solid solution) -> γ''(bct) DO_{22}-Ni_3Nb + γ'(fcc) $L1_2$-Ni_3Nb -> β(orthorombic) -> Widmanstatten structure.

Equilibrium orthorombic β phase formed through a grain boundary cellular reaction detected after 5 hours of aging or as Widmanstatten plates.

On continued aging at 973 K, and on aging at higher temperatures the γ" precipitates were found to be favourable nucleation sites for the γ' particles.

The precipitation of both γ' and γ" phases followed the Hagel-Beattie requirements for lattice mismatch, ie. γ/precipitate mismatch < 1 pct.

The e/a ratio, ie. the average per atom of the total number of electrons outside the inert gas shell, was used as a criterion to establish the formation and stability of the precipitating phases. The e/a ratio for the two phases were calculated using EDS microanalysis and was found to be in agreement with the Engel-Brewer correlations.

TABLE OF CONTENTS

LIST OF TABLES

LIST OF FIGURES

Chapter I

INTRODUCTION

In the past forty years the mechanism of precipitation and the accompanying changes in properties have been extensively investigated, particularly in aluminum alloys and steels; but less attention has been given to copper alloys. Lately the attractive diversity of properties obtainable by precipitation in copper alloys, seems to have warranted more detailed consideration.

A large amount of copper is used for tubing in water lines, for fuel and oil lines in aircraft radiators, heat exchangers, etc. Copper is also very resistant to corrosion and is the basis of many industrial alloys.

The high strength, very good resistance to sea water corrosion and weldability of Cu-30Ni alloys has accounted for their extensive use in marine environments.

The Cu-Ni binary alloy forms a continuous solid solution for all compositions, but the addition of small amounts of alloying elements such as Nb, Al and Fe produces a heat treatable material. Addition of these elements to the Cu-Ni matrix produces strengthening by the precipitation of the metastable Ni_3 (Nb, Al, Fe) γ', γ'' and β phases.

From the literature review in the next chapter, it is evident that very little work has been done to study the precipitation of γ' ($L1_2$) and γ'' (DO_{22}) precipitates in copper-base alloys and the potential strengthening and heat treatability that could be gained through it.

Recent investigations by Raghavan [12,13] show that Niobium additions to a Cu-30% Ni alloy promoted the precipitation of the γ''-DO_{22}-(Ni_3Nb) phase, while further additions of small amounts of aluminum promoted the γ'-$L1_2$-(Ni_3Nb) phase. It was suggested that this change in precipitate could be associated with the e/a "electron to atom" ratio of the precipitating compound.

Thorough investigations of nickel base and iron alloys strengthened by γ' and γ'' phases, suggest that other factors such as crystallography and lattice mismatch in addition to the e/a ratio, influence the formation of these phases. But still the factors affecting the stability and formation of these phases are not yet fully understood.

In view of this situation, it was decided to investigate the precipitation behaviour of a Cu-30Ni-2Nb-4Fe alloy on aging at 873, 973 and 1073 K. The criteria influencing the stability of the precipitating phases in light of the existing theories were investigated, and the mechanical properties of various aged specimens were also studied.

Chapter II

LITERATURE REVIEW

Various methods have been devised to strengthen metals. The ultimate objective is to bring the real strength as close as possible to the theoretical strength by either eliminating dislocations or creating as many barriers for dislocation motion as possible. The latter route is the one chosen in most strengthening mechanisms.

Precipitation of a second phase from a supersaturated solid solution is in practice, a very versatile and common strengthening technique.

In the context of this thesis, the theories explaining the mechanisms of nucleation and growth of these precipitates in a matrix will be reviewed in this chapter. Also a review of the precipitation process in Cu-Ni systems which are strengthened by γ' and γ'' precipitates will follow. Finally the morphology and characteristics of these two phases are discussed in light of the existing theories.

2.1 Precipitation in solid solution.

The decomposition of one phase into one or more phases, in solid state, by the precipitation process can be divided in three stages:

(i) the formation of nuclei of the new phase

(ii) the growth of these nuclei; and

(iii) the coarsening of the new phase without change in volume fraction.

Stage (i) may occur in two ways; if small concentration fluctuations occur spontaneously, the reaction can proceed by spinodal decomposition; but if all small fluctuations tend to decay, there is said to be a nucleation barrier which has to be overcome for successful nucleation to occur.

2.1.1 Nucleation from supersaturated solid solution.

At temperatures below the solvus curve a solid solution is no longer structurally stable and its free energy increases with a decrease in temperature. This increase in free energy can be reduced only if nuclei of a second phase are formed with a composition different than that of the matrix. These nuclei grow with time and the transformation of the solid solution proceeds by nucleation and growth. The nucleation process may be either homogeneous or heterogeneous.

Homogeneous nucleation is the process which occurs without the benefit of pre-existing heterogeneities in the system. This concept is illustrated by figure 1 which shows the change in free energy of the system with the formation and growth of a new phase within the system.

Curve A shows the increase in free energy which is due to the increase of the area of new surface, as a particle of the new phase grows. Curve B is the decrease in the volume free energy which occurs due to the replacement of the unstable matrix by the more stable phase of the growing particle. And curve C shows the rise in energy due to the misfit strain per unit volume (ΔGs) of the system, since the transformed volume will not fit perfectly into the space originally occupied by the matrix.

Summing all these contributions, the total free energy, represented by curve D will be [1]:

$$\Delta G = \Delta G_{volume} + \Delta G_{surface} + \Delta G_{strain}$$

$$\Delta G = -v\Delta Gv + A\gamma + v\Delta Gs$$

For a spherical shape nucleus of radius r:

$$\Delta G = -\tfrac{4}{3}\pi r^3 \Delta Gv + 4\pi r^2\gamma + \tfrac{4}{3}\pi r^3 \Delta Gs$$

$$\Delta G = -\tfrac{4}{3}\pi r^3 (\Delta Gv - \Delta Gs) + 4\pi r^2\gamma \qquad (1)$$

From this equation and figure 1 it can be seen that for a given treatment there is a certain radius of nuclei r*, at which a maximum occurs in the free energy curve.

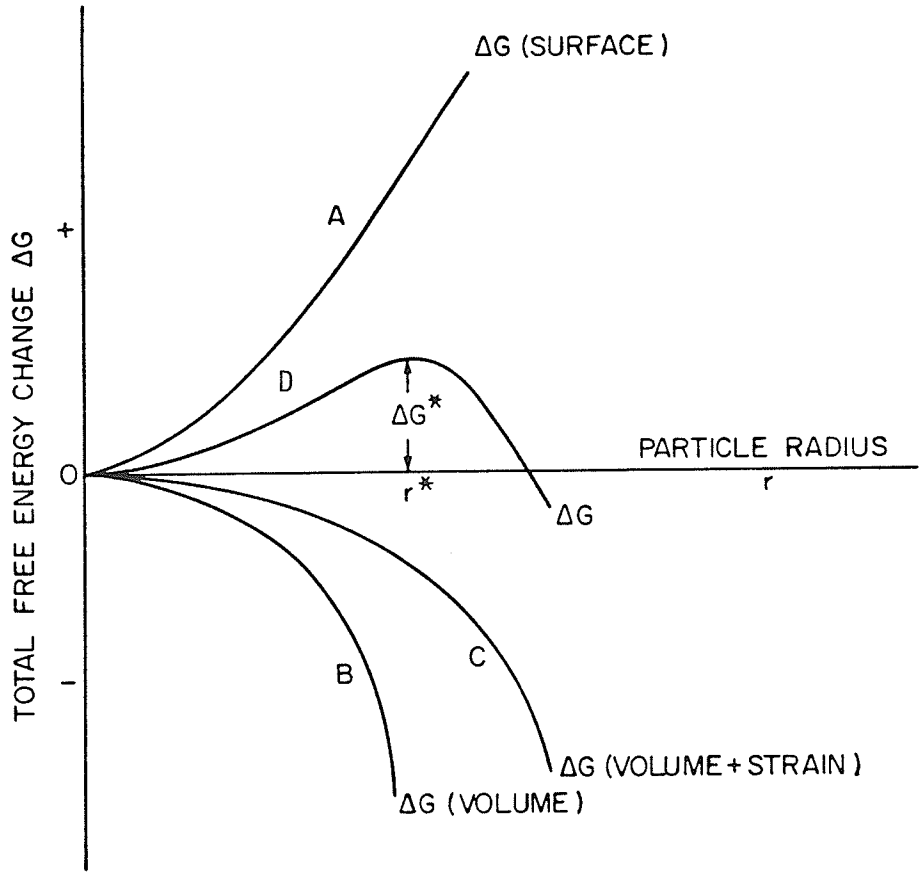

Figure 1. Relationship between total free energy change and particle size for a homogeneous nucleus [1,2].

If the radius of the nuclei is less than r* the system can lower its energy by their dissolution, whereas if r > r* the free energy of the system decreases if the nuclei grow.

If the slope of curve D is zero ($d\Delta G/dr = 0$) the equation yields $$r^* = \frac{2\gamma}{(\Delta Gv - \Delta Gs)}$$ and the corresponding critical free energy of activation for nucleation is given by [1]:

$$\Delta G^* = \frac{16\pi}{3} \cdot \frac{\gamma^3}{(\Delta Gv - \Delta Gs)^2} \qquad (2)$$

On average the number of nuclei of critical size is given by the Maxwell expression:

$$C^* = C_0 \exp(-\Delta G^*/kT) \qquad (3)$$

where, C_0 is the number of atoms per unit volume, k is the Boltzmann Constant and T is the absolute temperature. Thus the C* can be defined as the steady state nucleation rate or the number of stable nuclei produced in unit time, in unit volume of untransformed solid. But in order for the nuclei to reach a critical size it must be supplied with solute atoms which diffuse from the surrounding matrix. Therefore a diffusion term must be included in the nucleation equation, and the homogeneous nucleation rate will then be:

$$N(hom) = \omega \cdot C_0 \cdot \exp\left(-\frac{\Delta Gm}{kT}\right) \exp\left(-\frac{\Delta G^*}{kT}\right) \qquad (4)$$

where ω is a factor that includes the vibrational frequency of the atoms and the area of critical nucleus and, ΔGm is the activation energy for atomic migration.

In the above equation for nucleation rate it has been assumed that the nuclei are spherical, with equilibrium composition and of the same phase.

However, in practice nucleation will be dominated by whatever nucleus has the minimum activation energy barrier ΔG^*. Equation 2 shows that by far the most effective way of minimizing ΔG^* is by the formation of nuclei with smallest total interfacial energy. This criterion is dominant in the nucleation process. Incoherent nuclei have such a high value of γ that incoherent homogeneous nucleation is virtually impossible. If however, the nucleation has an orientation relationship with the matrix and coherent interfaces are formed, ΔG^* is greatly reduced and homogeneous nucleation process becomes feasible.

In most of the systems the precipitating phase and the matrix have such different crystal structures that it is impossible to form coherent low energy interfaces and homogeneous nucleation of the equilibrium phase. However it is possible to form a coherent nucleus of some other metastable phase which is not present in the equilibrium phase diagram. The most common example of this is the formation of GP zones. In Al-Cu alloys the first precipitate to nucleate is not θ but coherent Cu-rich GP zones. The reason for this can be explained in terms of the activation energy barriers for nucleation. GP zones are fully coherent with the ma-

trix, and thus have a very low interfacial energy, while the θ phase has a complex tetragonal crystal structure which can only form with high energy incoherent interfaces. In addition to this the GP zones minimize their strain energy by choosing a disc shape, with the C axis normal to the elastically soft <100> directions of the fcc matrix. Thus it is very easy for the GP zones to nucleate most rapidly.

The formation of GP zones is often followed by the precipitation of so called transition phases. The equilibrium θ phase in Al-Cu alloys is preceded by θ' and θ''. Figure 2 is a schematic free energy diagram for the above phases. The solubility of each phase at a given temperature is given by the common tangent construction ie. a_1, a_2, a_3, a_4. The transition phases θ' and θ'' are less stable than the equilibrium θ phase and have higher free energies as shown in figure 2. Transition phases form because, as GP zones, they have a lower activation energy barrier for nucleation than the equilibrium phase. Therefore the free energy of the alloy decreases more rapidly via the transition phases than by direct transformation to the equilibrium phase. Transformation stops when the minimum free energy equilibrium state G_4 is reached (fig. 2.) [1].

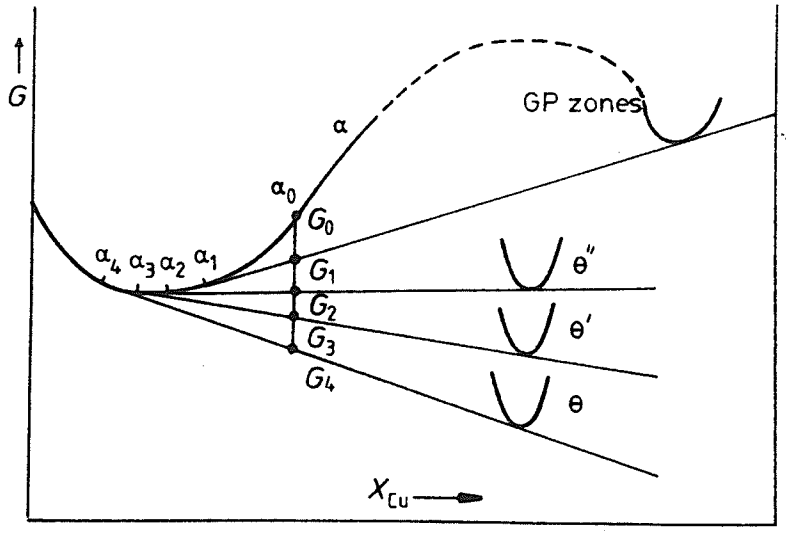

Figure 2. A molar free energy diagram for the Al-Cu system [1].

There are a few systems such as Cu-Co in which the equilibrium phase may nucleate homogeneously. However, nucleation in supersaturated solid solution is almost always heterogeneous. Suitable nucleation sites are defects such as excess vacancies, dislocations, grain boundaries, stacking faults, inclusions and free surfaces, all of which increase the free energy of the material. Such imperfections do not take part in the reaction, except to accelerate the precipitation which is already energetically favorable. The lattice imperfections have, therefore, come to be called "nucleation catalysts" and the total free energy for heterogeneous nucleation is [1,3]:

$$\Delta G(het) = -V\ (\Delta Gv - \Delta Gs) + A\gamma - \Delta Gd \qquad (5)$$

and the nucleation rate is given by:

$$N(het) = \omega .\ C.\ \exp\left(-\frac{\Delta Gm}{kT}\right) \exp\left(-\frac{\Delta G^*}{kT}\right) \text{ nuclei/m}^3\text{/sec} \qquad (6)$$

where C is the concentration of defects per unit volume, and ΔGd is the free energy released associated with the annihilation of a defect.

2.1.2 Growth of precipitates from supersaturated solid solution

Probably the most interesting stage of the precipitation process is the growth of stable nuclei into precipitate particles by the addition of solute atoms from the matrix. During growth, many factors come into play which combine to

determine the nature and orientation of the precipitate lattice; to determine which particles grow and their growth rate; to define the shape, array and population of the precipitate upon the properties of the alloy.

In the analysis of precipitate growth from supersaturated solid solutions, the possible limiting factors considered are the rate at which atoms are brought to or removed from the interface by diffusion, and the rate at which they cross the interface. The interface reaction is likely to be the rate limiting step during the early stages of growth since the diffusion distance tends to be zero in this situation. At large particle sizes, lattice diffusion is likely to be the slower step, since the continuous removal of solute from solution reduces the concentration gradient.

Diffusion controlled growth has been recently analysed in detail by Martin and Doherty [3]. For growth of spherical precipitates, the radius R after time t is given by [4]:

$$R = a(Dt)^{1/2} \qquad (7)$$

Where, D is the volume diffusion coefficient and a is the function of supersaturation. In the case of planar precipitates, a similar expression has been deduced [1].

$$S = a(Dt)^{1/2} \qquad (8)$$

Where S is the thickness of the precipitate.

Usually the crystal structure of the matrix influences the orientation of the particles of the new phase. There is

a tendency for the boundaries of the two phases to have similar atomic spacing and pattern (ie. matching or coherency) and this gives rise to geometric arrangement of precipitates known as widmanstatten structure. The orientation of the lattice in the new phase is related crystallographically to the orientation of the parent phase.

2.1.3 Overall transformation kinetics

The progress of an isothermal phase transformation can be represented by plotting the fraction transformation (f) as a function of temperature and time. A typical TTT diagram is shown in figure 3 [1].

Among the factors that determine f(t,T) are the nucleation rate, the growth rate, the density and distribution of nucleation sites, the overlap of diffusion fields from adjacent transformed volumes, and the impingment of adjacent transformed volumes.

The Avrami equation can be used to estimate the fraction transformed (f):

$$f = 1 - \exp(-kt^n) \qquad (9)$$

where, n is a numerical exponent with the values between 1 to 4; and provided there is no change in the nucleation mechanism, n is independent of temperature. The factor k depends on nucleation and growth and is therefore very sensitive to temperature.

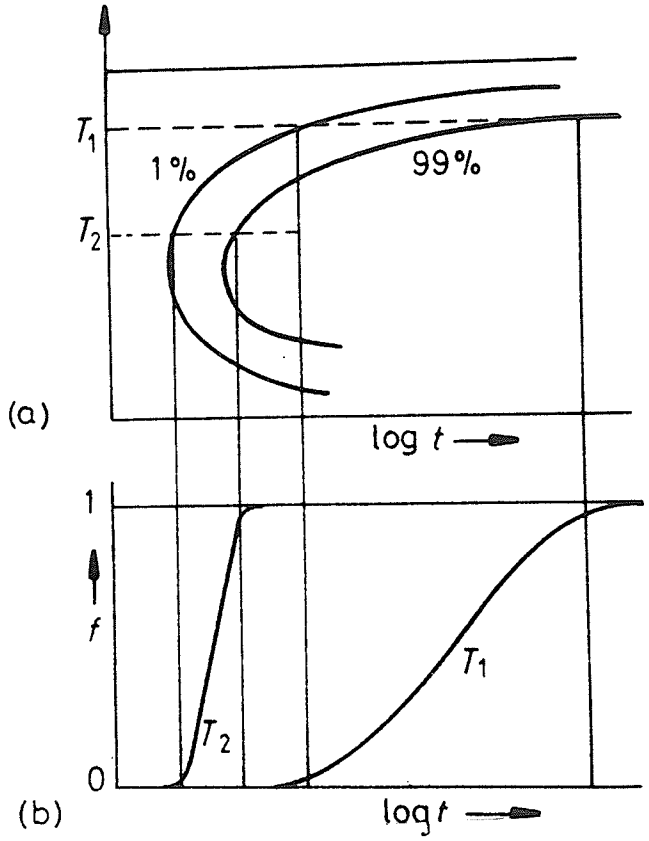

Figure 3. The percentage transformation versus time for different transformation temperatures [1].

2.1.4 Coarsening of particles.

The microstructure of a two phase alloy is always unstable if the total interfacial free energy is not at a minimum value. Therefore a high density of small precipitates will tend to coarsen into a lower density of large particles with a smaller total interfacial area.

Consider two spherical precipitates with different radii r_1 and r_2 as shown in figure 4*a*. Figure 4b shows that the solute concentration in the matrix adjacent to a particle will increase as the radius of curvature decreases. Therefore there will be concentration gradients in the matrix which will cause solute to diffuse in the direction of the largest particles away from the smaller ones, so that the small particles shrink and disappear while the larger ones grow. The overall result is that the total number of particles decreases and the mean radius increases with time.

So when precipitation from supersaturated solid solution is complete, further aging leads to precipitate coarsening driven by the interfacial free energy between the precipitate and the matrix. This process is known as Ostwald ripening. However, such coarsening often produces an undesirable effect on properties, such as loss of strength.

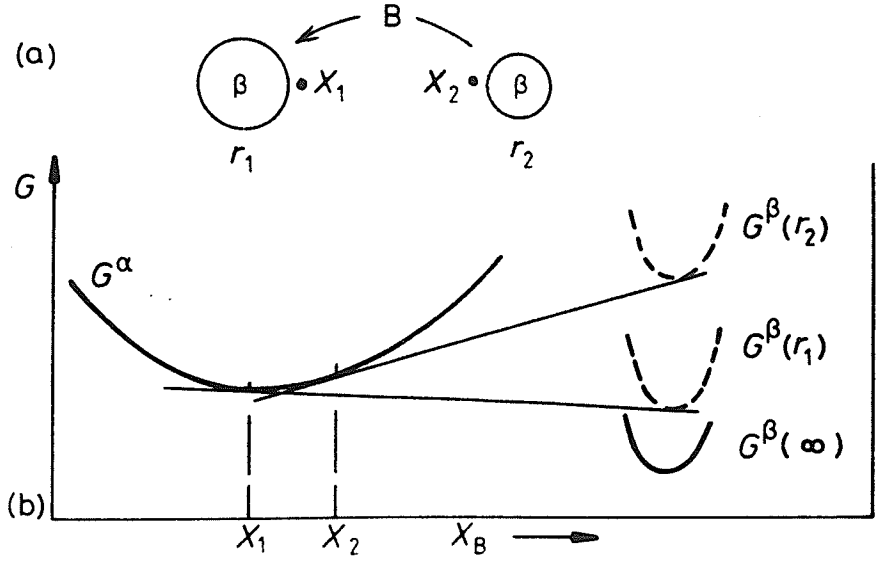

Figure 4. Schematic diagram showing the origin of particle coarsening; (a) two particles β with different radii r_1 and r_2, (b) the concentration of solute is highest outside the smallest particle [1].

The coarsening kinetics depend upon the rate controlling step in the process. If lattice diffusion is the rate controlling step, then the analysis of Wagner [5] and Lifshitz-slyozov [6] shows that the coarsening rate is given by the equation [4]:

$$\bar{r}_1^3 - \bar{r}_0^2 = 8\ D\ \sigma\ Vm\ C\alpha\ t/9\ R\ T \qquad (10)$$

Where,

$\bar{r}_1$ is the average particle radius at time t,

$\bar{r}_0$ is the average particle radius at time t=0,

D is the volume diffusion coefficient of the diffusing species,

σ is the specific surface free energy of the particle/matrix interface,

Vm is the molar volume of the precipitate,

$C\alpha$ is the equilibrium solute content in the matrix,

R is the gas constant,

T is the temperature in K.

2.2 The Cu-Ni alloys.

The substitution of copper atoms by nickel atoms in the lattice of copper results in a substitutional solid solution.

Nickel often exhibits bivalency while copper is often monovalent, but they both possess the same fcc structure. The difference in atomic radii is less than 3% (r(Cu) = 1.27 Å, r(Ni) = 1.246 Å) [7]. From the above statements and according to Hume-Rothery [8], complete solid solubility is expected in the Cu-Ni system. Figure 5 shows the phase diagram of this system [9]. Here, it can be seen that Cu and Ni form a continuous solid solution as expected.

There are many copper nickel alloys in use for industrial applications. Particularly the Cu-30Ni cupronickel is largely used for condenser tubes due to its corrosion resistance and because it is free of season cracking [10]. This cupronickel can be hot or cold rolled and is noted for its extreme malleability in cold weather. High strength alloys have been developed based on 70/30 Cu/Ni with the addition of about 0.7 Si or 1.3 Nb. The addition of a few percent iron (1 to 2) to these Cu-Ni alloys, increases the resistance to corrosion, especially to impigment attack in fast moving sea water [10].

2.3 The Cu-30Ni alloy with Nb and Al additions.

Except for the early work of Smith [11], only two attempts have been made to investigate the precipitation of metastable Ni_3Nb precipitates in Cu base alloys and the potential strengthening that could be derived through these precipitates.

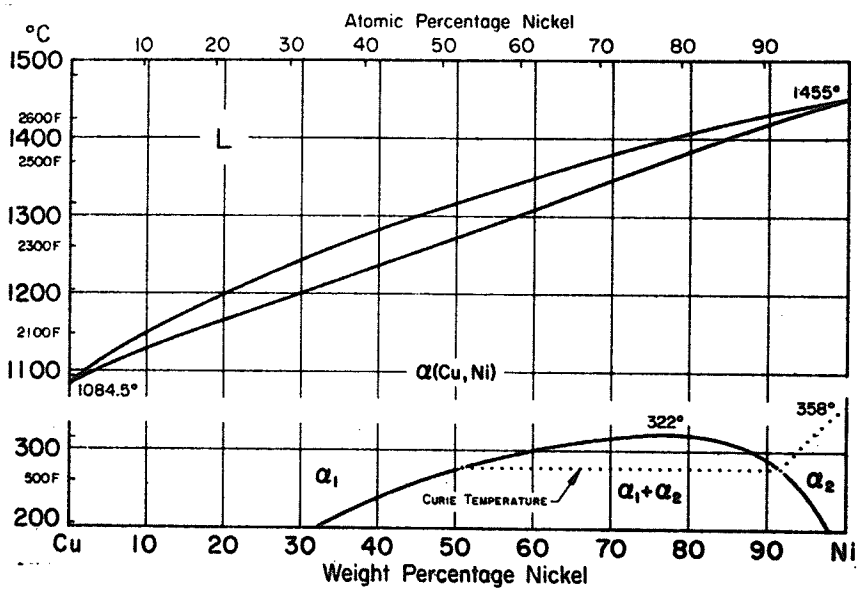

Figure 5. The Cu-Ni phase diagram [9].

The solubility of iron in copper is small but it can increase to several percent at 1343 K [7]. The solid solubility of niobium in copper is also limited, and it increases significantly in Cu-Ni alloys. Specifically niobium can reach to 2.7 Wt% in a Cu-30Ni matrix at 1373 K [11].

It was found [11,12] that additions of 1 and 2.5 pct niobium in a Cu-30Ni alloy resulted in the precipitation of body centred tetragonal, metastable Ni_3Nb γ" precipitates on the {100} matrix planes. These γ" precipitates transformed to the equilibrium β phase with prolonged aging at higher temperatures.

Addition of 2.2 pct aluminium resulted in the formation of spherical γ'-$L1_2$ (Ni_3Nb) type precipitates at all the aging conditions. But when the percentage of aluminum was decreased to 1.1, γ' particles that formed during the initial stages of aging coexisted with random platelets of γ" which seemed to be replaced by the β phase on continued aging [13].

The importance of the γ' and γ" phases based on the composition Ni_3 (Nb, Al, Ti), may be seen when one examines the alloy systems that are being strengthened by these phases.

2.4 Alloy systems with γ' and γ'' precipitates.

Several high strength nickel and iron base alloys are known to be strengthened by the metastable phases γ' and γ'' whose composition is based on the Ni_3 (Nb, Al, Ti) formula [14-19].

Particularly the 718 nickel base superalloy has been the subject of numerous investigations [20-24]. These reports were conflicting and could not establish the nature of the strengthening phase. The similarity of the crystal structures of γ' and γ'' made this identification very difficult by conventional methods.

In 1969 Paulonis et. al. [20] were able to differentiate between γ' and γ'' using centered dark field and electron diffraction techniques in a TEM.

Quist et. al. [25] studied the influence of iron and aluminum on the precipitation of the metastable Ni_3Nb phases in the Ni-Nb system and reported on the requirements for the formation of these phases.

Most recently, the precipitation in Cu-30Ni-Nb with Aluminum additions alloy was studied [12,13]. Some of the factors affecting the formation of γ' and γ'' were examined and will be reviewed in a later section.

But still the factors affecting the formation and stability of the γ' and γ'' phases are not clearly understood, which presents a great obstacle in the development of alloys strengthened by these phases.

The possibility of producing suitable age hardening alloys for marine applications using the alloy based on 70/30 Cu/Ni, and a better understanding of the factors affecting the formation of γ' and γ'', that will assist in the development of new alloys, have prompted the present work.

2.5 Crystal structure and orientation relationship of the γ' and γ'' phases.

The unit cells for the γ' and γ'' structures are shown in figure 6 [26]. The γ' has a fc cubic ($L1_2$) structure while the γ'' has a bct (DO_{22}) structure.

The lattice parameter for the fcc ($L1_2$) is 3.589 Å and the lattice parameters for the bct (DO_{22}) are $a_o = b_o =$ 3.624 Å, c = 7.406 Å and c/a = 2.044. These parameters are reported [25] for the Ni_3Nb composition.

The γ'' precipitate forms as discs on the {100} planes, and the crystallographic orientation between the fcc matrix and the precipitate as determined by electron diffraction is:

{100} matrix // (001) γ'' (DO_{22}).

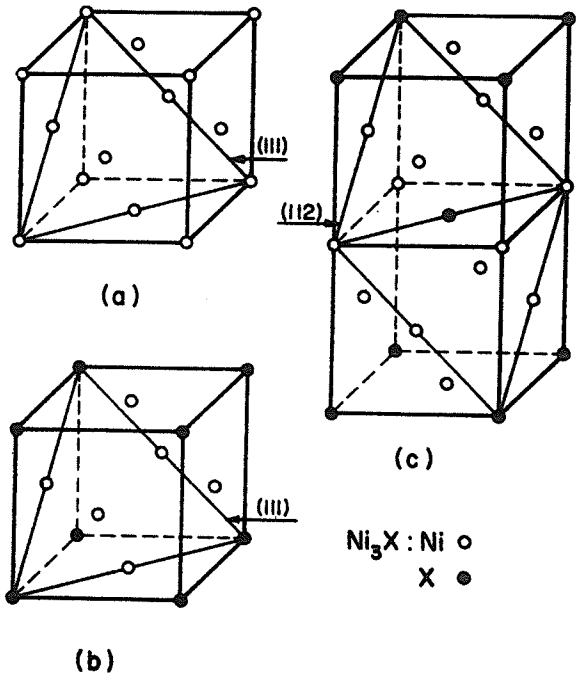

Figure 6. Unit cells of [a] Al (fcc), [b] $L1_2$ (γ') and [c] DO_{22} (γ'') structures [26].

<100> matrix // [001] γ" (DO_{22}).

As for the γ' in a fcc matrix the crystallographic relationship is:

{100} matrix // {100} γ' ($L1_2$).

<100> matrix // <100> γ' ($L1_2$).

The structures of γ' and γ" can be formed by stacking identical close packed ordered layers of the A_3B composition. These layers are analogous to the {111} planes of the fcc structure. In the fcc γ' and the bct γ" phases, B atoms are located at the corners of equilateral triangles and rectangles respectively as shown in figure 7 [26].

The influence of several variables on the stacking sequence of A_3B structures has been studied by various investigators [25-28].

It can be seen from figure 6 that the DO_{22} γ" unit cell consists of two fcc γ' unit cells stacked one above the other. Except for the slight distortion along the aγ" axis and the higher one along cγ" axis the two phases represent ordered variations of the fcc lattice.

2.5.1 Morphology of γ' and γ".

The shape of the individual γ' particles was found to vary from perfectly spherical to perfectly cubical [29]. Intermediate shapes have also been reported.

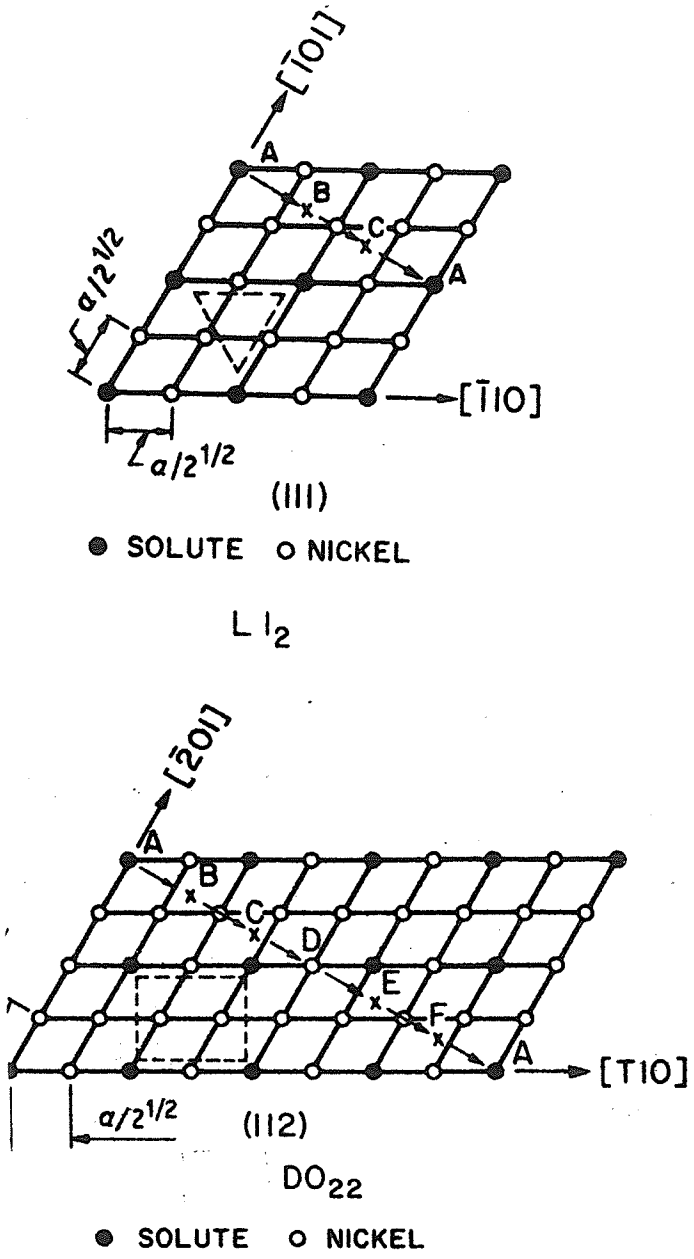

Figure 7. Ordering and stacking sequence in $L1_2$ and DO_{22} compounds based on the Ni_3X formula [26].

Hagel and Beattie [30] have suggested that the form of the γ' precipitates appears to be related to γ'/matrix, lattice mismatch. According to this report spheres are formed when the lattice misfit between γ' and matrix is less than 0.5 percent, and cubes are formed if the misfit is in the range of 0.5 and 1.0 percent.

Other investigation [31] in a Nimonic alloy has shown that a cubical γ' morphology existed even when the misfit was less than 0.1 percent. This suggests that the Hagel and Beattie observation was only partially correct.

Others [32], suggest that γ' particles which are spherical when small, usually take a cubical shape when they grow in size.

The shape of the γ'' phase is known to take a disc shaped morphology [20].

2.6 Factors influencing the formation of γ' and γ''.

The occurrence and stability of the γ' and γ'' phases have been widely studied. From various investigations [25,33] it has been concluded that a number of interdependent factors influence the formation of these phases. The most important of these factors are:

2.6.1 Crystallographic considerations.

It has been shown by Quist et al [7,25] that additions of fcc or hcp component in fcc matrix will promote the formation of γ'-$L1_2$ phase. Also addition of bcc component that has an allotropic form of fcc or hcp at some temperature, to a fcc matrix again induces the precipitation of the $L1_2$ phase. Thus the influence of Al or Nb additions to a fcc matrix may be explained according to the above crystallographic considerations, since Al (fcc) promotes the formation of γ'-$L1_2$ phase, while Nb (bcc) induces the precipitation of the γ''-DO_{22} phase.

It is important to note that the $L1_2$ phase has never been reported to form in any binary system containing only fcc and bcc elements.

2.6.2 Lattice mismatch.

It has been suggested that coherent precipitation of γ' type phases will be inhibited if the lattice mismatch between the precipitate and the matrix exceeds 1.0 percent [30].

Quist et. al. [25] have verified this theory in their investigation of the metastable phases in the Ni-Nb system.

They found that approximately 12.0 percent niobium should be added to nickel in order to expand the lattice parameter of the solid solution to values approximating those of γ' and γ''. According to their findings precipitation of these phases occured only when niobium reached 10.0 pct.

Additional evidence for the importance of lattice mismatch is provided by reports on the Inconel 718 alloy [25]. Here it is shown that the presence of 20 percent of chromium and 20 percent of iron, together with small additions of other alloying elements has expanded the a_0 to 3.60 Å This value is well within the limits of 1.0 percent of the lattice parameters of γ' and γ''.

The substitution of various elements for A and B in γ' and γ'' (A_3B) phases influence their lattice parameters and as a result of this the degree of misfit between matrix and precipitate is altered.

The degree to which these lattice constants are affected by the substituting elements depends on whether substitution occurs for the A or the B atom in the A_3B structure, because of the difference in their atomic radii.

A review [26] on the role of the alloying elements on Ni_3X phases provides detailed information on the effects of alloy substitution on the mismatch parameter.

2.6.3 (a) Free electron concentration.

In addition to crystallographic and lattice mismatch considerations, it has been shown [20-21] that the e/a ratio could also serve as a powerful criterion for predicting the stability of the $L1_2$ and DO_{22} structures.

Sinha [27,28] has studied the influence of the electronic concentration of the intermetallic compounds upon their structure. He found that the e/a ratio of the compound plays an important role in controlling the type of crystal structure.

Later work [34], indicated that the γ' phase is stabilized when its e/a < 8.65 and the γ'' phase is stabilized when its e/a > 8.65. The e/a ratio is defined as "the average per atom of the total number of electrons outside the inert gas shells".

The electron concentration in Ni_3X type compounds and their components are shown in Table 1, [26]. This information can be used to predict the stability of phases in various alloys.

In the Cu-Ni-Nb system precipitation of β and γ'' phases are known to occur [12]. Here partial substitution of nickel by copper in Ni_3Nb will increase its e/a ratio and therefore stabilize the γ'' phase. In the same alloy, addi-

TABLE 1

The e/a ratios, in Ni_3X type compounds [26].

Element (X)	(e/a) in element	Structure of the Ni_3X type compound	Average (e/a) in the compound
Al	3	$L1_2$	8.25
Ti	4	DO_{24}	8.5
V	5	DO_{22}	8.75
Nb	5	Cu_3Ti (type)	8.75
Ta	5	Cu_3Ti (type)	8.75
Ga	3	$L1_2$	8.25
In	3	DO_{19}	8.25
Si	4	$L1_2$	8.5
Ge	4	$L1_2$	8.5
Sn	4	DO_{19}	8.5
Cr	6	---	---
W	6	---	---
Fe	8	---	---
Co	9	---	---
Ni	10	---	---

tion of aluminium will reduce the e/a ratio since aluminum can substitute for Nb and the corresponding e/a ratio for aluminum is only 3 as compared with 5 for niobium (Table 1). Therefore when the percentage in aluminum is low, γ'' is stabilized; but when the percentage is increased the e/a ratio is reduced and γ' is stabilized.

2.6.3 (b) Engel Brewer considerations.

According to the principles of Engel and Brewer [35] the number of s and p valence electrons determine the crystal structure of an element, compound or solid solution. Bcc structures are stable for e/a ratios < 1.5, hcp structures are stable for e/a between 1.75 and 2.25, and the fcc structures are stable at 3.0.

The change in the stabilities of crystal structures with increase in the (s+p) electron concentration is shown in figure 8 [26].

The influence of iron in γ' and γ'' formation can be predicted using this theory. In a Ni-Nb alloy, iron behaves as fcc since the matrix is fcc [25]. Substitution of Ni by Fe would not change the Ni_3Nb precipitate stability. But if fcc iron with an (s+p) value of 3 substitutes for bcc niobium which has an (s+p) value of 1.5, it will result in an increase in the (s+p) electron concentration in Ni_3Nb. Thus,

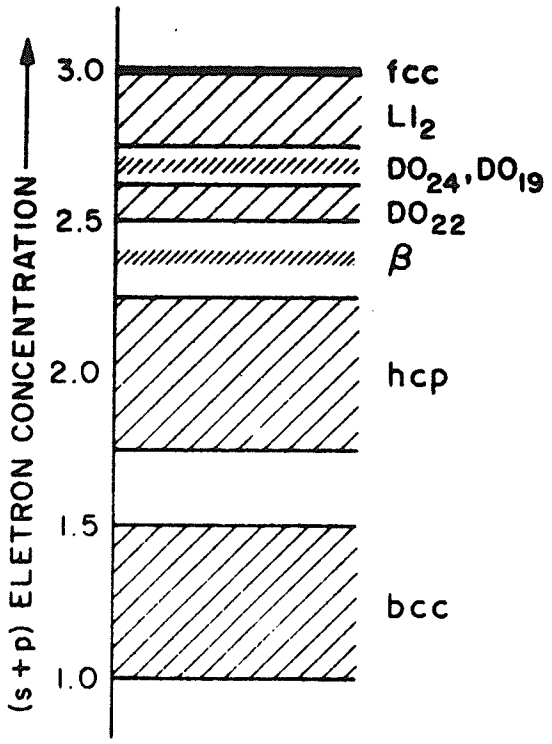

Figure 8. A schematic diagram showing the change in the stabilities of crystal structures with increase in the (s+p) electron concentration [26].

according to figure 8, addition of Fe would induce the precipitation of γ".

2.7 The β phase.

The γ' phase (Ni_3Nb) is a metastable phase which overages to the orthorombic β (Ni_3Nb) phase [25]. This β phase is the equilibrium phase of Ni_3Nb.

In nickel and iron base alloys, the β phase precipitates via either of two discontinuous reactions [16,36], a cellular reaction initiating at the grain boundaries or it can form as a transgranular widmanstatten precipitate in the matrix along {111} γ planes with the following crystallographic relationship [9].

$$(010)\beta \;//\; (111)\gamma$$
$$[100]\beta \;//\; (1\bar{1}0)\gamma$$

It has been shown that in niobium containing Cu-Ni alloys the onset of the formation of the β phase corresponded to the initiation of softening during aging. Thus, it is important to establish the characteristics of the transformation sequence of the strengthening precipitate to the orthorombic phase, since it produces an undesirable degradation of the properties of the material.

On continued aging of the same alloy, the β phase gave rise to a widmanstatten structure.

Chapter III

EXPERIMENTAL PROCEDURE

3.1 Preparation of the alloy.

A 200 gram melt was prepared in an induction furnace under a flowing Argon atmosphere. The composition of the alloy was: Cu - 30Wt% Ni - 2Wt% Nb - 4Wt% Fe.

The purity of the alloying elements was:

Cu - 99.95 Wt%

Ni - 99.95 Wt%

Nb - 99.80 Wt%

Fe - 99.95 Wt%

This melt was used for hardness testing, x-rays and microstructural changes.

Three additional melts of 450 grams each, and of the same composition were made by the same method, in order to study the tensile properties of the alloy.

3.2 Processing and heat treatment.

The ingots were homogenized at 1373 K for 48 hours. Specimens for hardness testing, optical metallography and x-ray diffraction were rolled to about 3.5 mm, and specimens for TEM studies were rolled to a thickness of 0.22 mm. The melts used for tensile specimens were rolled to 1.4 mm thickness by a rigorous thermo-mechanical treatment. All these materials were given a final solution treatment at 1373 K for 1 hour, followed by water quenching. The solution treated specimens were aged at various temperatures for different lengths of time. For all heat treatments, specimens were encapsulated in Vycor tubes under a 10^{-4} mm pressure of Hg.

3.3 Mechanical testing.

Flat tensile specimens with a thickness of about 1.3 mm were prepared. The gauge length of the specimens was 20 mm and the gauge width was 5 mm.

All specimens were tested in uniaxial tension at room temperature using an Instron machine at a constant strain rate of 8.3×10^{-4} sec^{-1}.

The 0.2 pct yield stress, ultimate tensile strength and total elongation to fracture were determined and were plotted against aging time at 873 and 973 K.

Hardness measurements were taken with a Vickers hardness tester, using a load of 5 kg. Seven measurements were taken for each sample and the mean value was determined. The HV was plotted against aging time at 873 and 973 K.

3.4 X-ray diffraction analysis.

The precipitation sequence during aging was examined by X-ray diffraction. A Philips X-ray diffractometer and a 114.6 mm Debye-Scherrer camera were used for identifying precipitating phases and measuring changes in lattice parameters and diffraction patterns. Cu radiation with Nickel filter and Cr radiation with vanadium filter were used and the films were exposed for 4 hours.

The Debye-Scherrer samples were cut longitudinally from the strip material and electropolished to approximately a cylindrical shape. All other aged and as quenched specimens were electropolished to remove surface oxides or other contaminants [37,38].

Low speeds were selected on the Philips diffractometer (1/4 $^{o}2\theta$ per minute) over a scanning range of 10 to 140 $^{o}2\theta$ values.

The intensities of the reflections on the Debye-Scherrer films were estimated visually. The (420) high angle reflection was employed in conjuction with the Straumanis method [39] for precise lattice parameter measurements. In some cases the lattice constants were obtained by extrapolating against the Nelson-Riley function [40].

3.5 Electron Microscopy.

Thin foils for electron microscopy were prepared using a jet electropolishing unit. The electrolyte used was a solution of 2:1 methanol:nitric acid by volume. The temperature of the solution was maintained between -30 to -40 ^{o}C. A potential of 15 volts along with a current of about 90 to 100 mA and were used as the electropolishing conditions. After polishing, the discs were washed in ethanol and methanol solutions.

The thin foils were examined in a Philips 300 transmission electron microscope operated at 100 kv.

Aged samples were used to prepare carbon extraction replicas. These samples were etched in a solution of either nitric acid with water or HNO_3:CH_3COOH:acetone in equal proportions in order to reveal the precipitates. It was then shadowed with a light film of carbon under a 10^{-4} mm Hg

pressure. The specimens were etched again in the same solution and the carbon replicas were stripped. The carbon films were collected on copper grids for TEM studies. For EDS analysis they were placed on carbon coated nylon grids.

3.6 Scanning electron microscopy and EDS analysis.

Etched samples were mounted on aluminum holders and their microstructre was examined in a JEOL 840 scanning electron microscope, equipped with an EDS x-ray energy analyzer.

Carbon extraction replicas on carbon coated plastic or Be grids were placed on a graphite holder (low background) and were examined with the EDS x-ray analyzer in order to establish the elemental composition and distribution of the precipitate particles.

All analyses were carried out at 25 kv with a fixed probe current of 200 pA. A machine dead time of approximately 30% was maintained and the acquisition time was 120 seconds.

Microanalysis at ten different locations of each sample was conducted and the results were averaged.

X-ray energy spectra were generated and the intensities were obtained by integrating kα x-ray peaks using a Tracor Northern data processor, after background was subtracted.

Pure standards were used to determine a series of k values for each element relative to Si [41].

Correction factors were used to compensate for absorption and fluorescence as proposed by others [42,43].

Chapter IV

EXPERIMENTAL RESULTS

4.1 Hardness measurements.

The Vickers hardness of the specimens aged at 873 and 973 K was measured after quenching from the aging temperature. The variation in hardness with aging time is shown in figure 9. It is seen that aging at 873 K produced a steady increase in hardness which leveled off after about 150 hours to a value of about 200 VPN. This is about 100% greater than the hardness of the solution treated specimen which was 102 VPN. At this temperature, overaging was not evident even after 1500 hours of aging treatment.

On aging at 973 K the hardness increased rapidly to attain a peak value of about 230 VPN after five hours of aging. This value of hardness was maintained for about 40 hours and it then decreased slowly up to 750 hours which was the longest time for which the alloy was aged at this temperature.

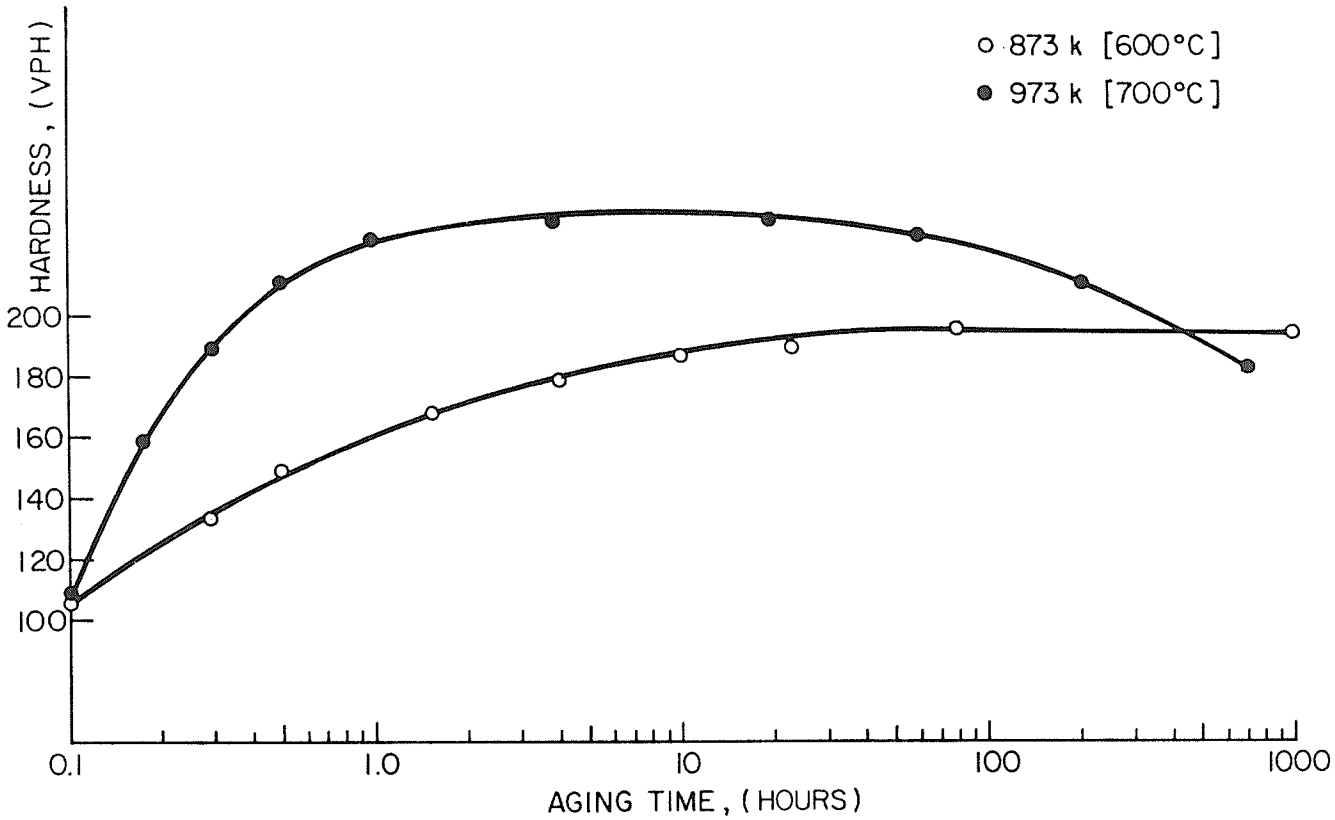

Figure 9. Effect of aging on the hardness values (VPH) of the alloy, aged at 873 K and 973 K.

4.2 Tensile properties.

The variation in 0.2 pct yield strength (YS), ultimate tensile strength (UTS) and pct elongation with aging time at 873 and 973 K are shown in figures 10 and 11 respectively.

Both figures illustrate a classical aging behavior which is in good agreement with the hardness-aging time curves shown in figure 9. During the early stages of aging, the variation in strength and ductility follow the normal behaviour ie. as aging time increases, strength also increases and ductility decreases.

On aging at 873 K, the strength increased slowly up to about 150 hours of aging, where it started leveling off. An increase of 250 MPa in YS, 200 MPa in UTS and a reduction of 40% in total elongation were observed at this aging temperature.

At 973 K the peaks of the curves were displaced towards lower aging times. Maximum strength was observed at an interval of 2 and 30 hours. The strength increased to a peak value of 580 MPa (YS), 750 MPa (UTS) and then decreased on continued aging.

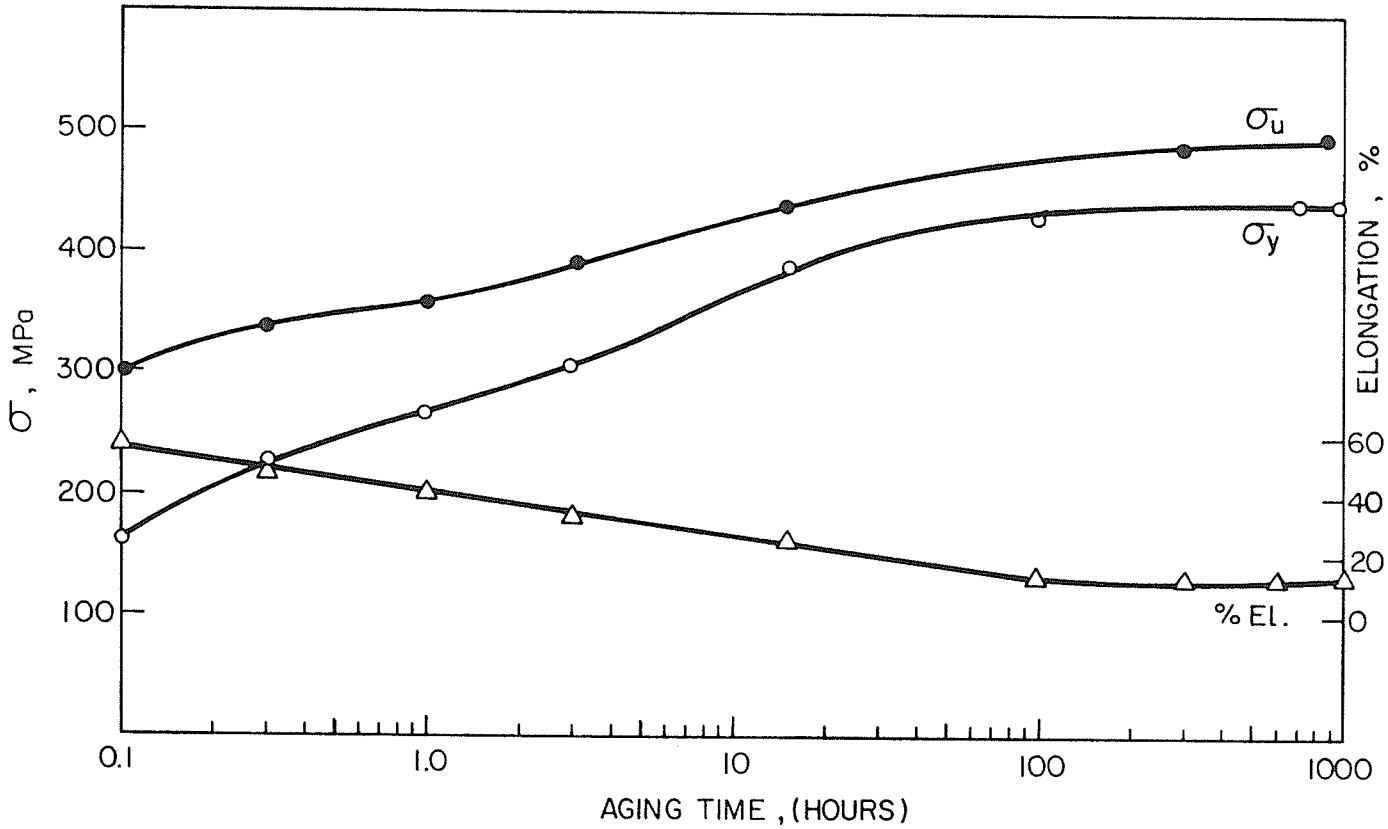

Figure 10. Effect of aging on the mechanical properties of the alloy, aged at 873 K.

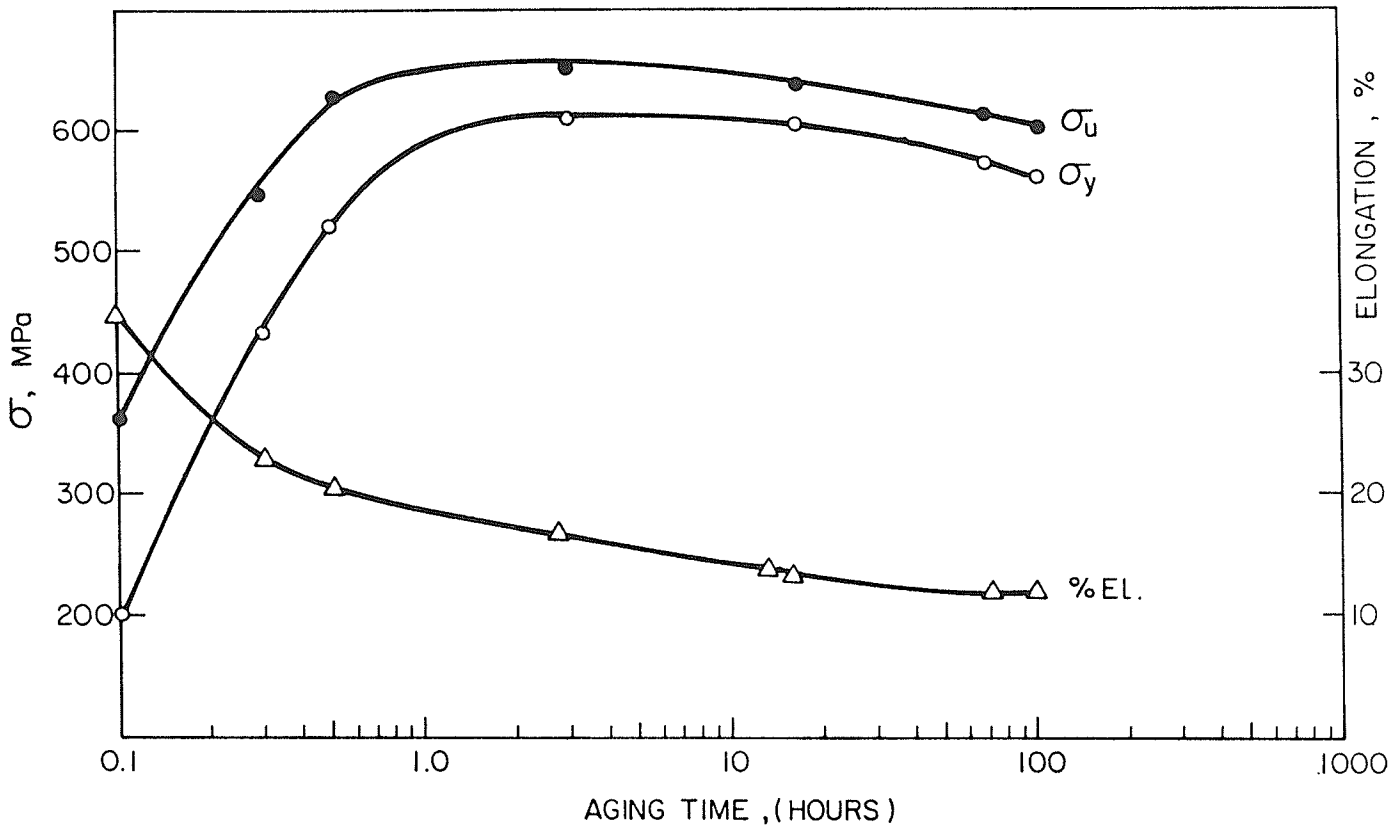

Figure 11. Effect of aging on the mechanical properties of the alloy, aged at 973 K.

4.3 X-ray diffraction analysis.

X-ray diffraction studies of aged specimens were carried out to measure the variation in lattice parameters of the matrix with aging, and to detect any superlattice peaks due to precipitates.

The lattice parameters of the γ matrix was measured using the (420) high angle reflection on the powder film, employing the Straumanis method [39]. For the Debye-scherrer powder diffraction technique, Cu-Ni filtered radiation was used, which was generated from a tube under a voltage of 40 kv and a current of 20 mA. The exposure time for all films was 4 hours.

The matrix was identified as fcc solid solution, and The variation of the lattice parameter of the matrix $a\gamma$, with aging time is shown in Table 2. The results show a very slight decrease in $a\gamma$ from 3.590 Å in the solution treated condition to 3.587 Å on aging at 973 K as shown in Table 2. There does not seem to be any significant variation in lattice parameter as shown in Table 2.

Bulk, electropolished aged samples of the alloy were also examined with the x-ray diffractometer, for the detection of second phase reflections. Cu-Nickel filtered and Cr-Vanadium filtered radiation were used.

Table 3 presents the x-ray diffraction data obtained from a specimen aged at 973 K for 2 hours. It is seen that only a limited number of secondary peaks appeared on the chart. These peaks can arise from both γ'(fcc) and γ''(bct) phases since both structures represent ordered variations of the fcc lattice. The (111) reflection was the most prominent at both 873 and 973 K at various aging times. The absence of extra peaks may be due to the fact that the precipitates are too small and their volume fraction is very low.

TABLE 2

Variation in the Lattice parameter of γ matrix.

(Cu-Ni filtered radiation)

Treatment	$a_0(\gamma)$ in Å
Sol. treated	3.590
873 K 30 min	3.590
873 K 15 hrs	3.588
873 K 140 hrs	3.590
973 K 700 hrs	3.587
1023 K 9 hrs	3.589

TABLE 3

X-ray diffraction data of specimen aged at 973 K for 2 hours. (Cu-Ni filtered radiation)

d	I	Suggested phase	(hkl)
2.25		NbC	
2.10	50	γ' or γ''	(111) or (112)
2.078	100	γ	(111)
1.970		Unidentified	
1.797	65	γ and γ' or γ''	(200)
1.268	69	γ and γ'	(220)
1.086	80	γ and γ'	(311)
1.036	40	γ	(222)
0.895	10	γ	(400)
0.823	60	γ	(331)
0.802	10	γ	(420)

4.4 Electron microscopic studies.

The microstructural development on aging was followed mainly by electron microscopy, since optical metallography could not reveal any structural changes. The precipitation reactions and the hardening phases were identified, and the growth and stability of these phases are described below.

4.4.1 Microstructure of solution treated specimen.

The microstructure of specimens, solution treated at 1100°C for 1 hour was examined using the electron microscope. A typical bright field image is shown in figure 12. The as quenched structure showed signs of precipitation and it appears to be a modulated structure.

A selected area diffraction pattern is shown in figure 13. This diffraction pattern only shows the matrix reflections and no secondary spots are present. This SADP can be indexed on the basis of the fcc crystal structure as shown in figure 13. Therefore, it is concluded at this stage that the alloy is single phase solid solution with an fcc crystal structure as determined by x-ray diffraction studies.

Some undissolved particles remained in the matrix, an example of which is shown in figure 14.

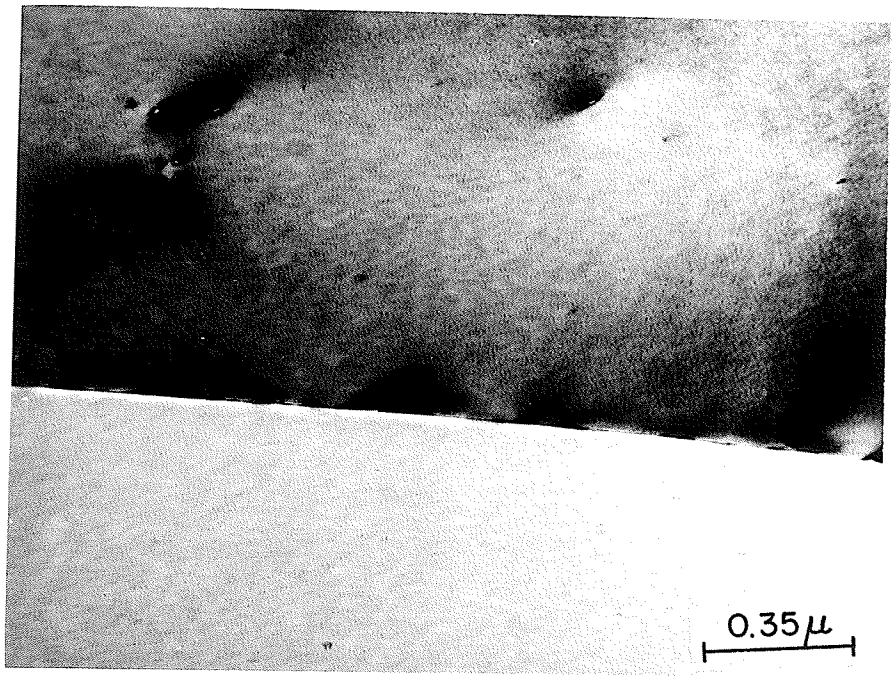

Figure 12. Microstructure of a solution treated specimen, annealed at 1373 K for 1 hour and water quenched.

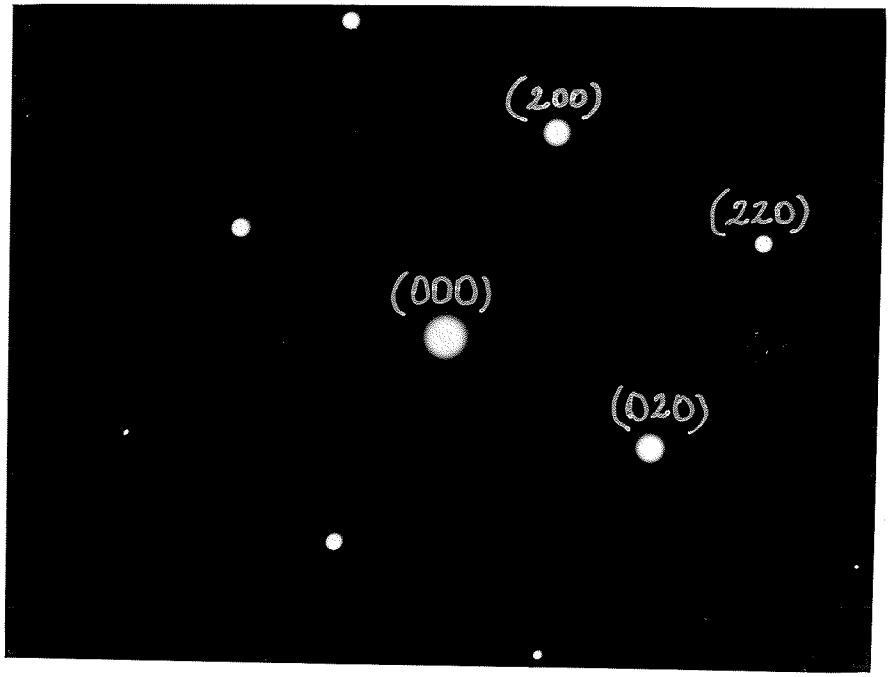

Figure 13. Diffraction pattern of a solution treated specimen. B=[001].

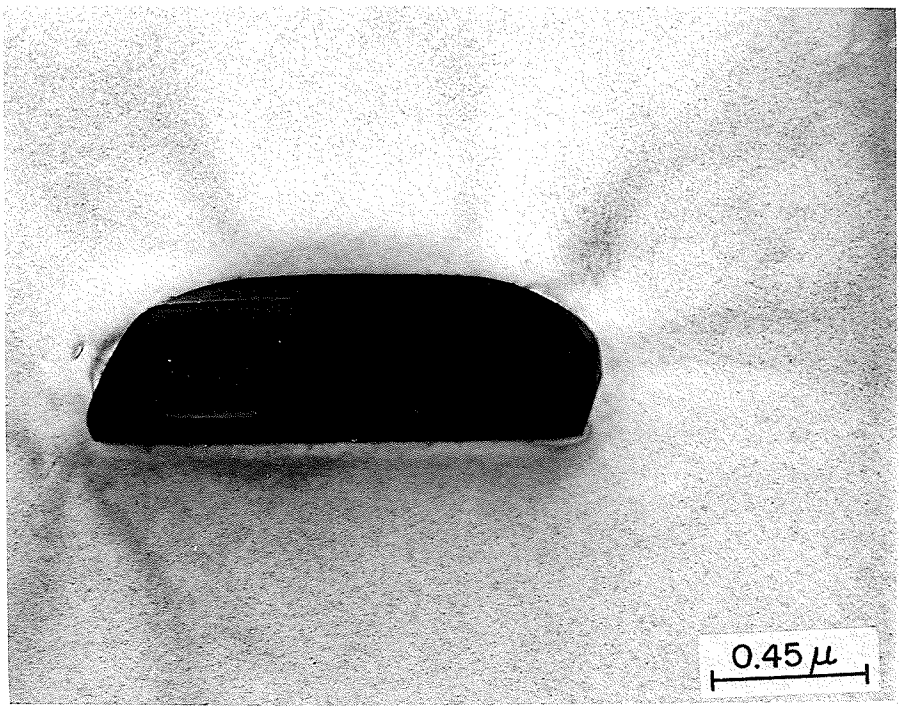

Figure 14. Solution treated specimen, showing an undissolved particle.

4.4.2 Microstructure on aging at 873 K.

The identification of the second phase particles could not be carried out with x-ray diffraction. For this reason, electron microscopy using thin film and carbon extraction replica techniques were employed.

4.4.2.1 Carbon extraction replica.

Precipitates of samples aged at 873 K for various times were extracted on carbon film which was collected on 200 mesh copper grids. Examination of these replicas in the microscope revealed fine precipitates distributed homogeneously throughout the matrix. All replicas revealed the same type of precipitate even after 1500 hours of aging. Figure 15, is a micrograph of a sample aged at 873 K for 140 hours. The precipitates appear dark on a white background. The shape of the particles is spherical, as shown in figure 15b.

The interplanar spacings of the precipitates were calculated using the camera constant method which was determined with an aluminum standard. The intensities of the reflections were estimate visually.

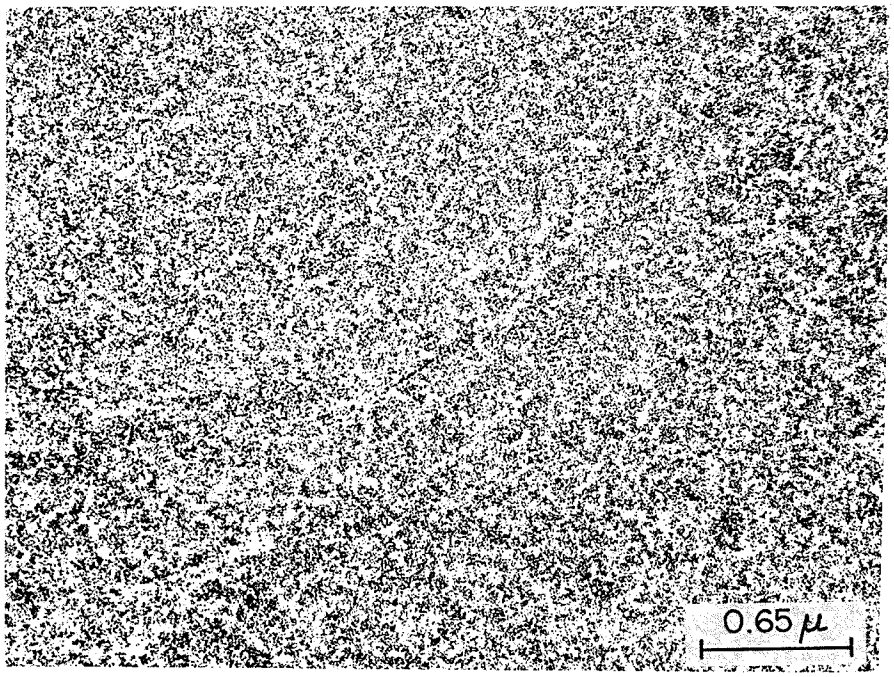

(a)

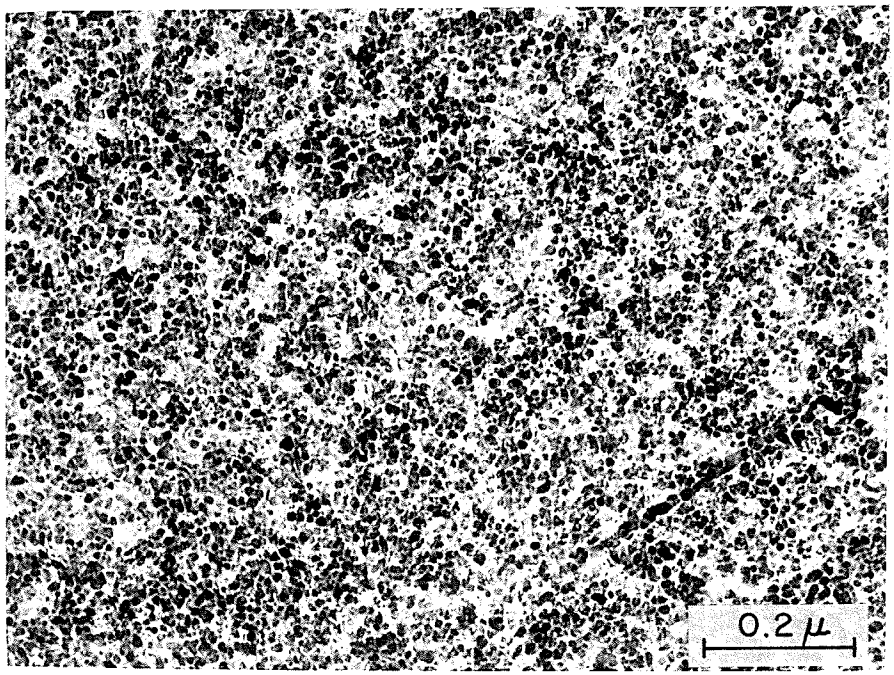

(b)

Figures 15 a and b. Carbon extraction replica of the alloy aged at 873 K for 140 hours. Spherical γ'-$L1_2$ particles are seen in figure 15 b.

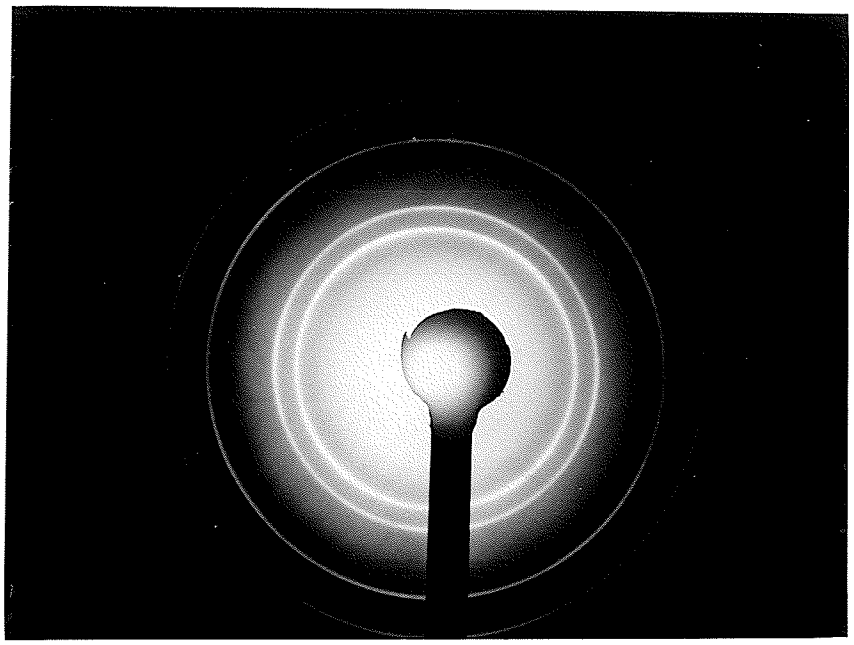

Figure 16. Ring pattern of precipitates shown in figure 15.

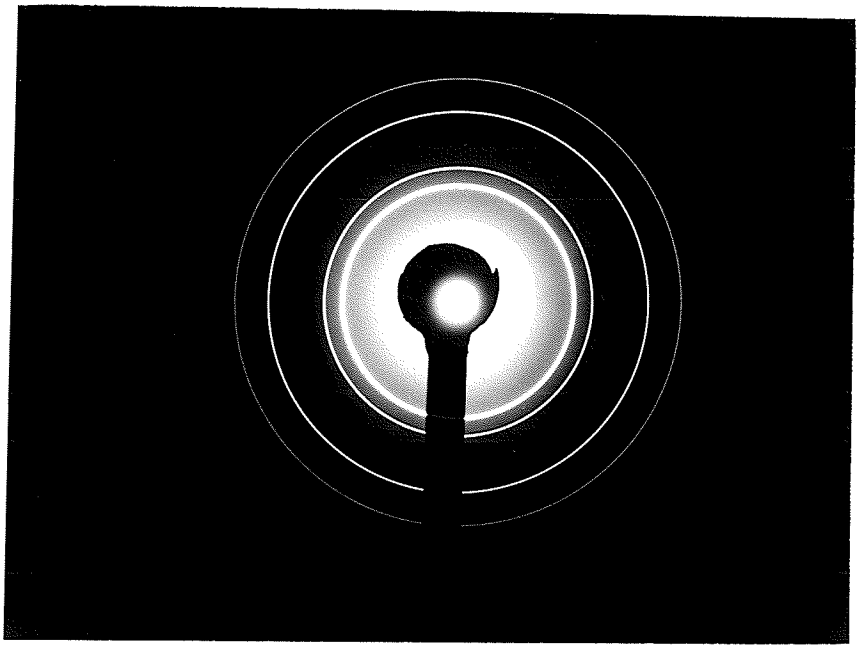

Figure 17. Ring pattern of an aluminum standard.
Camera constant = 5.304.

The ring pattern, of the precipitate replica shown in figure 15 and the corresponding ring pattern from an aluminum standard are shown in figures 16 and 17. The measurements and calculations resulting from these two patterns are listed in Table 4. The d-spacings and the intensities match closely with those of γ'-$L1_2$-Ni_3Nb phase, which suggests that the precipitates in a specimen aged for 140 hours at 873 K are of the γ'-$L1_2$ phase. Even after 1500 hours of aging at 873 K only γ' precipitate particles were identified.

4.4.2.2 Thin film microstructures at 873 K.

Optical metallography revealed no precipitation on aging up to 60 hours, but thin film electron microscopy of the alloy aged for 30 minutes showed a fine, modulated structure indicating initiation of decomposition. Aging for one hour produced secondary reflections on a [001] SADP (figure 19). The indexing of this diffraction pattern and the identification of the precipitate based on the occurrence of these extra precipitate reflections was carried out using the camera constant method and the ratio method. In this particular diffraction pattern, the matrix reflections can be indexed as fcc, and the precipitates as belonging to the γ'-$L1_2$-Ni_3Nb crystal lattice.

TABLE 4

Ring pattern analysis of figures 15 and 16.

Camera constant = $R \cdot d = \lambda L = 5.304$ cm-Å

2R	I	d	phase	(hkl)
2.56	vvs	2.072	γ'	(111)
2.96	vs	1.792	γ'	(200)
4.20	vs	1.263	γ'	(220)
4.92	vs	1.079	γ'	(311)
5.16	vw	1.029	γ'	(222)
5.95	vvw	0.891	γ'	(400)
6.51	ms	0.814	γ'	(331)
6.70	ms	0.791	γ'	(420)
7.36	w	0.720	γ'	(422)
7.83	w	0.677	γ'	(430)

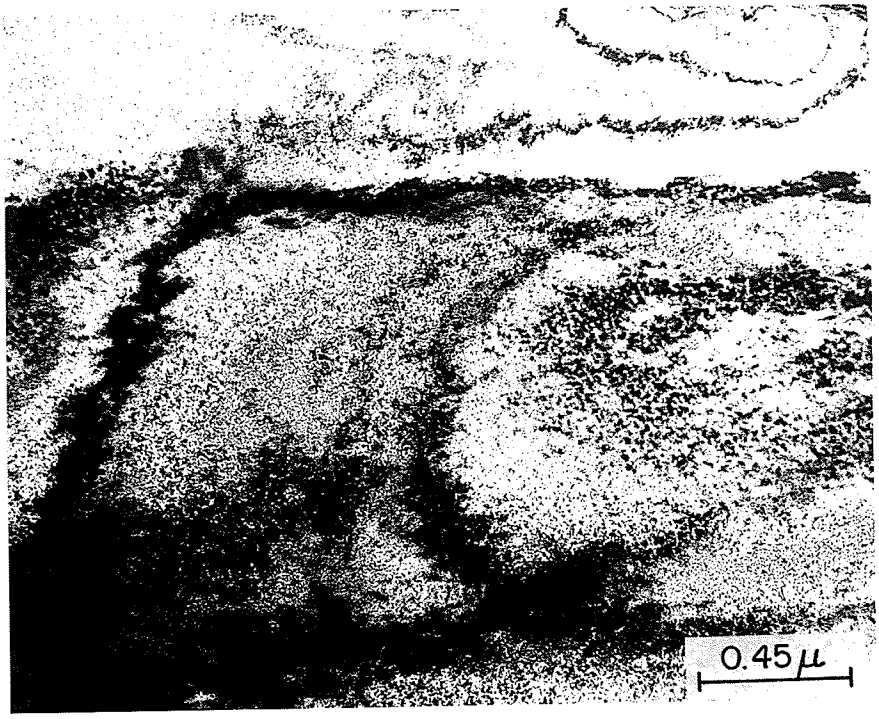

Figure 18. Microstructure of the alloy aged at 873 K for 1 hour.

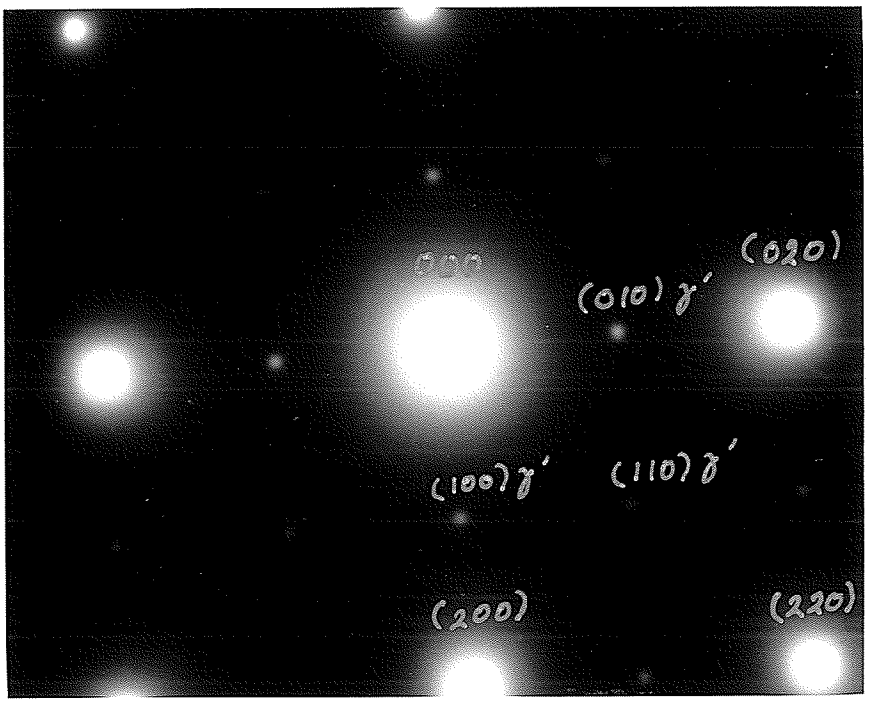

Figure 19. SADP of figure 18.

However individual precipitates could not be clearly resolved due to overlapping strain field of the particles, (figure 18).

Aging for 140 hours caused very little coarsening of the precipitates and it was possible to resolve them in bright field as shown in figure 15b. Figure 20 is a bright field of a specimen aged for 1000 hours. The precipitates have coarsened considerably as can be seen, and they seem to align themselves in the <100> directions. The SADP of the above bright field is the same as the one shown in figure 19.

The precipitates were identified as coherent fcc γ'-$L1_2$-Ni_3Nb particles. The shape of all the γ' precipitates is seen to be spherical in the initial stages of aging (figure 15b), but most of them develop a cuboidal shape as time progresses (figures 21 & 42). The particle size increased with time, but no discontinuous transformation was observed up to 1500 hours of aging (figure 23).

Streaking of the superlattice reflections was also not evident, indicating there is no trace of the disc-shaped γ'' bct precipitate.

There does not seem to be any precipitation reaction at the grain boundaries even after prolonged aging time. But a γ' free zone about 0.27 μ wide, adjacent to the boundaries was observed, in specimens aged for 1000 hours, (figure 22).

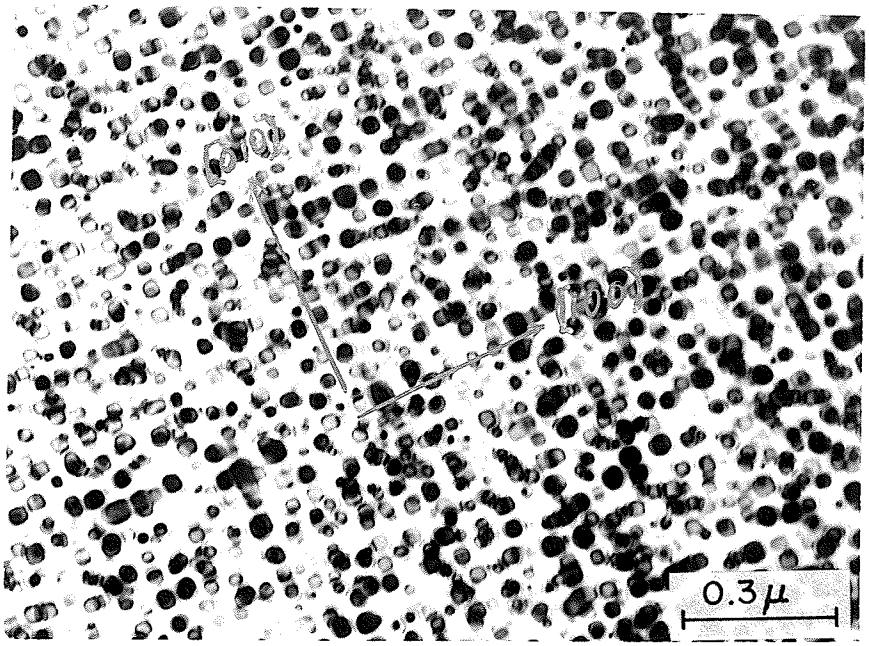

Figure 20. Micrograph of the alloy aged at 873 K for 1000 hours.

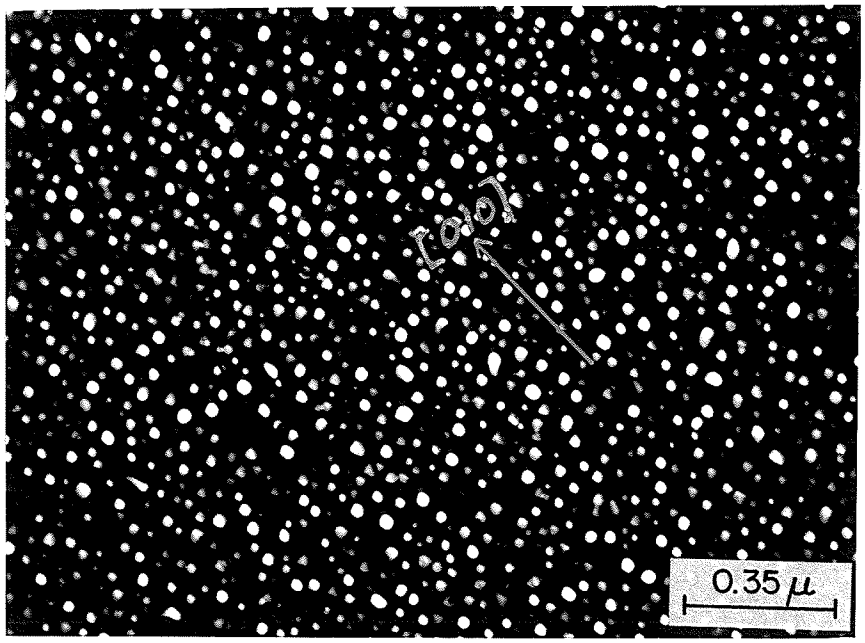

Figure 21. Dark field micrograph of figure 20 imaged with (100) γ' reflection; cubical shape of the γ' ($L1_2$) is seen.

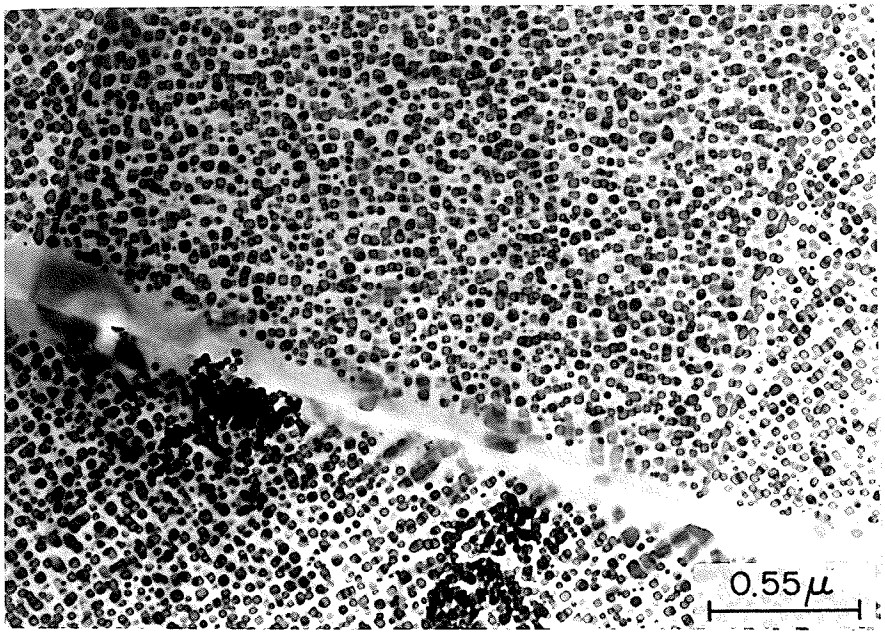

Figure 22. Specimen aged for 1000 hours at 873 K showing the precipitate free zone at the grain boundary.

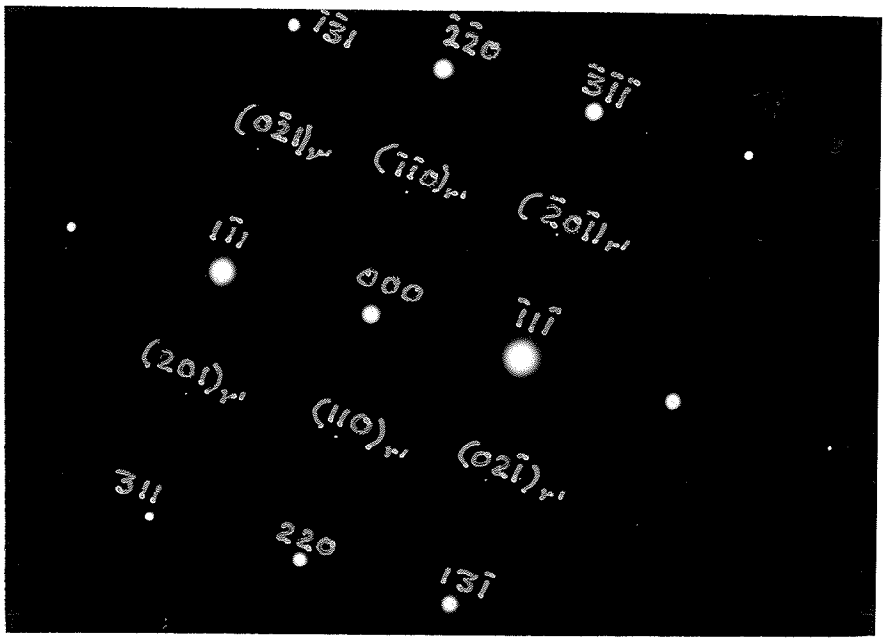

Figure 23. Diffraction pattern of the alloy aged at 873 K for 1500 hours. The ordered fcc γ' ($L1_2$) is still the precipitating phase. B=[112]

4.4.3 Microstructure on aging at 973 K.

On aging at 973 K the microstructural features were different from those at 873 K. Due to the high density of the precipitates and the excessive strain contrast around the particles, the strengthening phase could not be resolved in thin film bright field TEM studies. For this reason, further analysis using carbon extraction replicas and the unique technique employing electron diffraction and dark field (as described by Paulonis), had to be used.

4.4.3.1 Carbon extraction replica.

Precipitates were extracted from various specimens aged at 973 K. Figures 24 and 25 show the precipitate particles of such specimen aged for 2 hours. From these micrographs it can be seen that disc shaped particles are present. With some careful observation a number of spherical precipitates may be also seen. The ring pattern of these precipitates was obtained and the analysis of the results is listed in Table 5. The observed intensities and d-values matched well with the theoretical values of the γ"-DO_{22}-Ni_3Nb phase. The d-spacings from three of the rings could be matched with those of the γ' phase. But their intensities were very weak

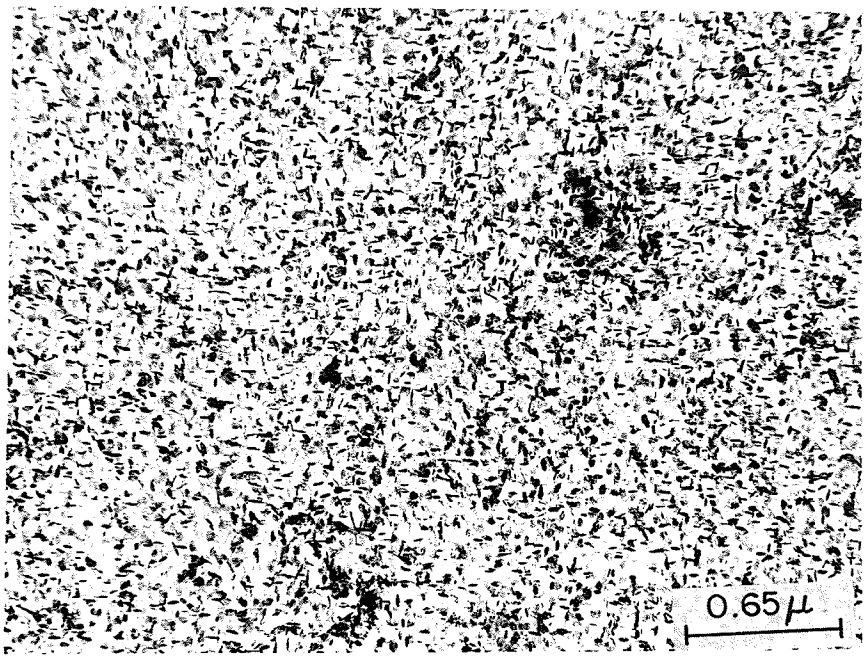

Figure 24. Carbon extraction replica of a specimen aged at 973 K for 2 hours.

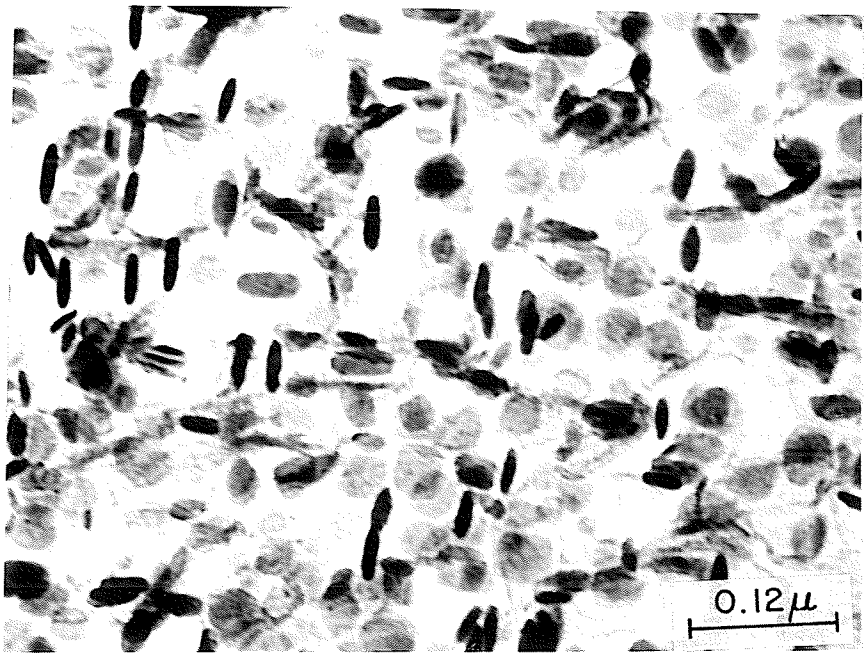

Figure 25. Same as figure 24 but at higher magnification.

as compared to others, which could be attributed to differences in chemistry that affect the electron diffraction structure factor and also to the low volume fraction of the γ' phase.

From these results we can definitely suggest that the γ''-DO_{22}-Ni_3Nb phase is present and some γ' precipitates may also exist in specimens aged at 973 K.

TABLE 5

Ring pattern analysis of figure 24.

$Rd = \lambda L = 5.3037$ cm-Å

R	I	d	Phase	(hkl)
1.62	vw	3.270	γ''	(002)
2.08	vw	2.550	γ''	(110)
2.51	vs	2.109	γ''	(112)
3.27	vw	1.619	γ''	(202)
4.11	w	1.289	γ''	(220)
4.19	ms	1.080	γ'' or γ'	(303) or (311)
5.12	vw	1.036	γ'	(222)
5.97	w	0.895	γ'	(400)
6.57	ms	0.807	γ'	(420)

4.4.3.2 Thin film microstructure at 973 K.

Thin foils of heat treated sample at 973 K were examined by electron microscopy. Figure 26 shows a bright field of a specimen aged at 973 K for 25 hours. The diffraction pattern of this area is shown in figure 27, with a beam axis [001] normal to the thin foil. The superlattice reflections are clearly visible. Quist et. al. [25] have studied the reciprocal space patterns in close-packed fcc matrix planes of a typical nickel base alloy containing the γ' or γ'' Ni_3Nb precipitates and their results are schematically shown in figure 28. Comparing the [100] fcc patterns of this chart with the [001] diffraction pattern of figure 27, it may be concluded that the fcc matrix contains the γ''-DO_{22} phase. But if the γ'' phase is present in a matrix, there are no unique secondary reflections for the γ' phase, and thus dark field images should be used to show if γ' is present.

The [001] diffraction pattern has been indexed in figure 29. The (100), (010), and (110) reflections can arise from either γ' or specific variants of γ''. The reflections indexed as $(1\frac{1}{2}0)$ and $(\frac{1}{2}10)$ can only be produced by the [010] and [100] variants of the bct γ'' phase respectively. This bct γ'' precipitate may form with its c axis along any of the three <100> fcc directions. The (100) and $(\frac{1}{2}10)$ reflections are streaked in the [100] fcc C direction, while the (010)

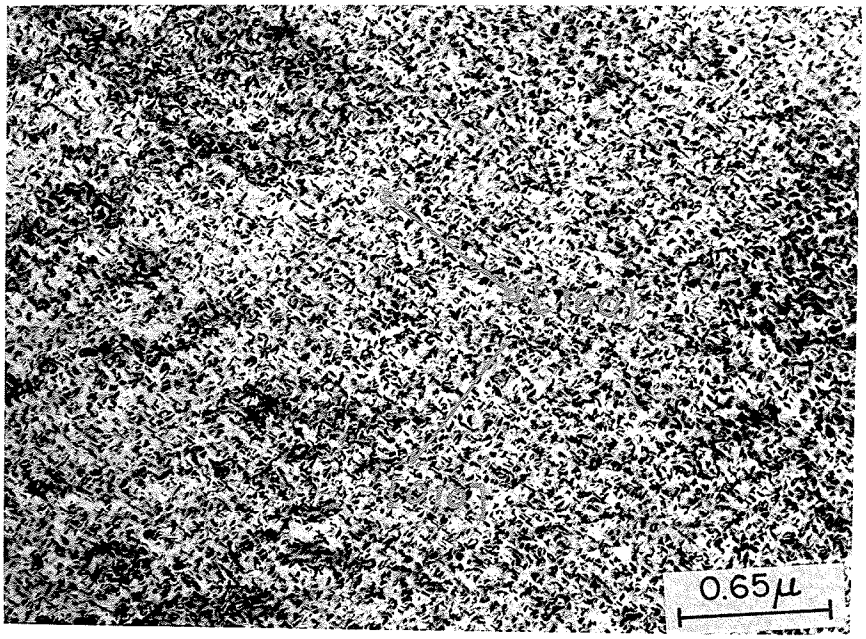

Figure 26. Microstructure of the alloy aged at 973 K for 25 hours.

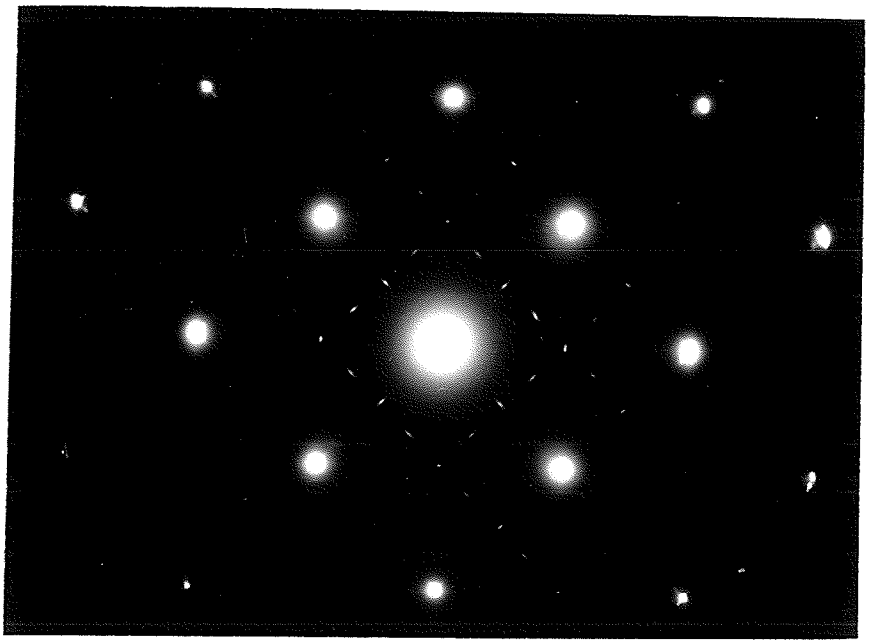

Figure 27. Electron diffraction pattern of figure 26, showing the existance of bct (DO_{22}) phase. B=[001].

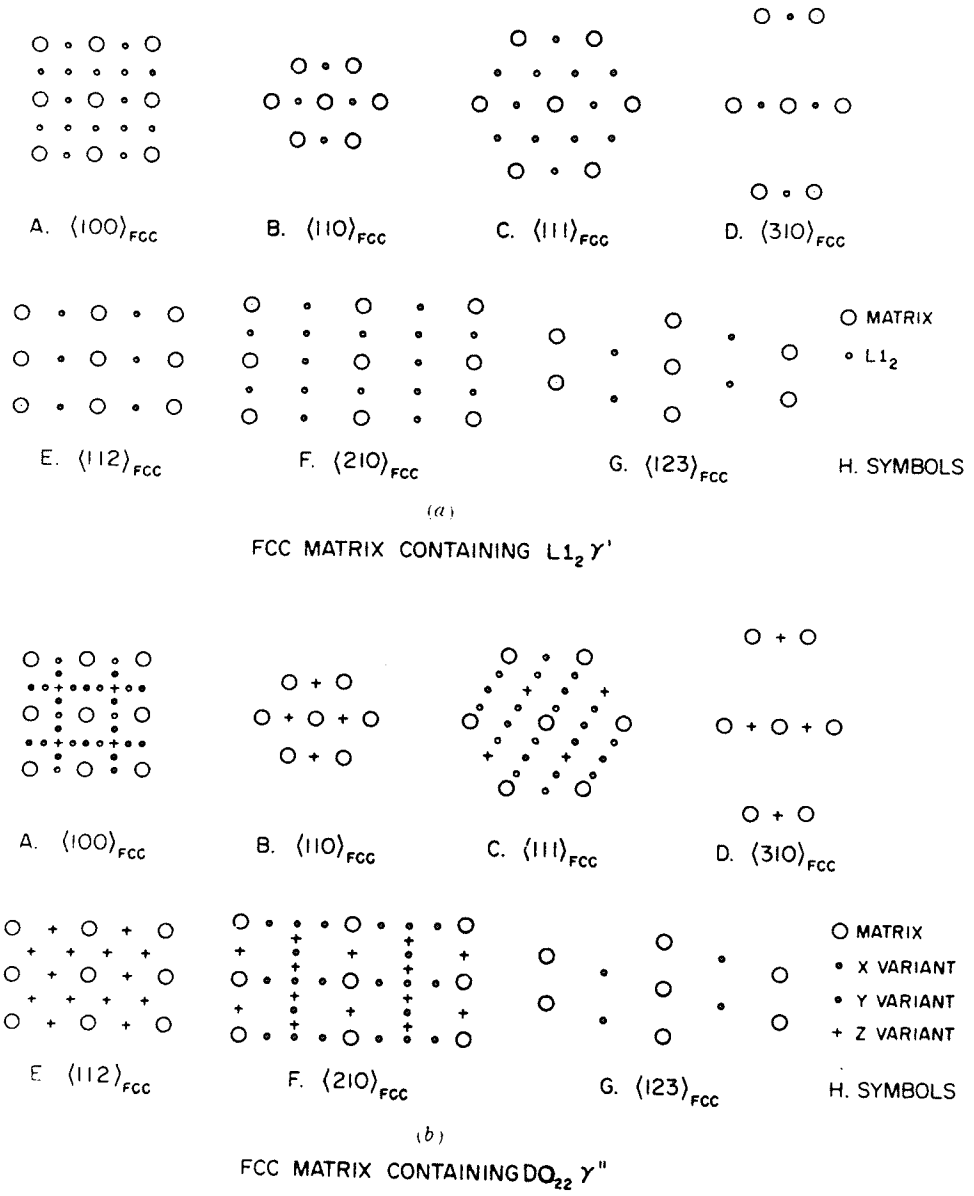

Figure 28. Schematic representation of close-packed planes in reciprocal space for a typical nickel-base fcc lattice containing (a) fcc $L1_2$ Ni_3Nb γ' and (b) bct DO_{22} Ni_3Nb γ'' [25].

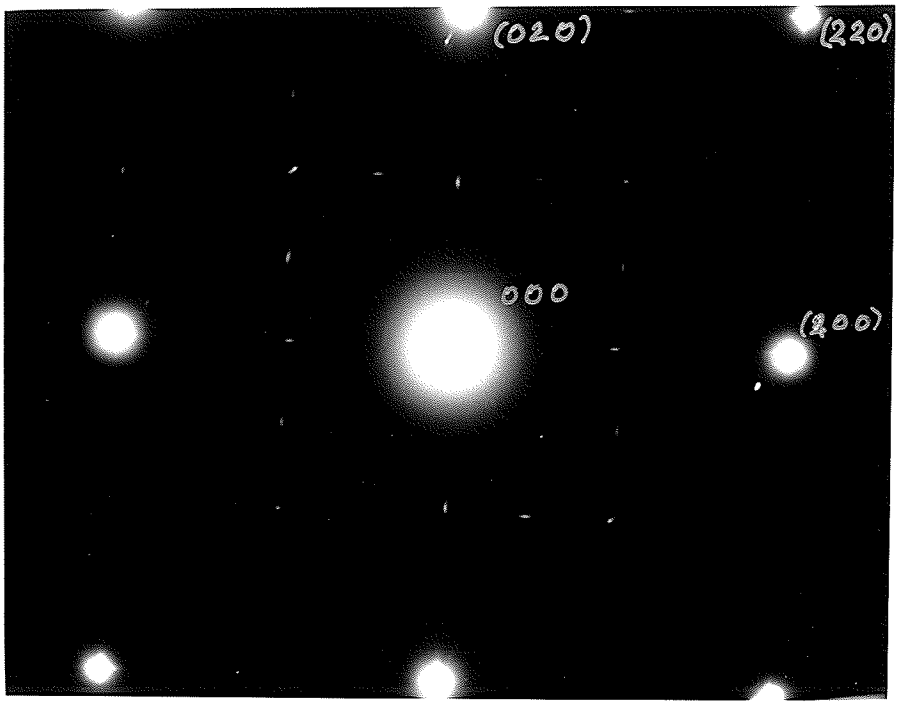

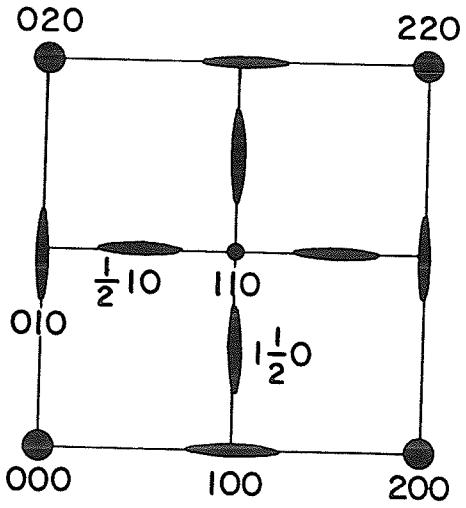

Figure 29. Indexed diffraction pattern of figure 27.

and $(1\frac{1}{2}0)$ are streaked in the [010]. For the (110) reflection there is no streaking observed since the corresponding [001]fcc C axis is normal to the pattern.

The streaking of these superlattice reflections suggests that the γ" has a disc-shaped morphology with the C axis being normal to the plane of the disc, which is in agreement with earlier observations [20,25].

Figure 30 shows a series of centered dark field micrographs corresponding to the bright field shown in figure 26. Figures 30a and 30b have been imaged with the $1\frac{1}{2}0$ and $\frac{1}{2}10$ reflections, therefore allowing only the γ" precipitates to be visible. The dark field imaged with the 110 reflection is shown in figure 30c and both γ' and γ" precipitates are observed.

Electron diffraction analysis using the camera constant method indicated that the lattice constants of the γ"(DO_{22}) phase were:

$a_0(\gamma") \sim 3.620$ Å, $C_0(\gamma") \sim 7.389$ Å and $(C_0/a_0) = 2.038$

On breaking the [001] diffraction pattern, into three precipitate zones and measuring the spacing of the precipitate reflections and the parallel matrix reflections it can be concluded that γ/γ" misfit is mainly in the direction normal to the plate (parallel to the c axis). It is estimated to be about 2.81 pct in the c axis direction and 0.82 in the plane of the plate.

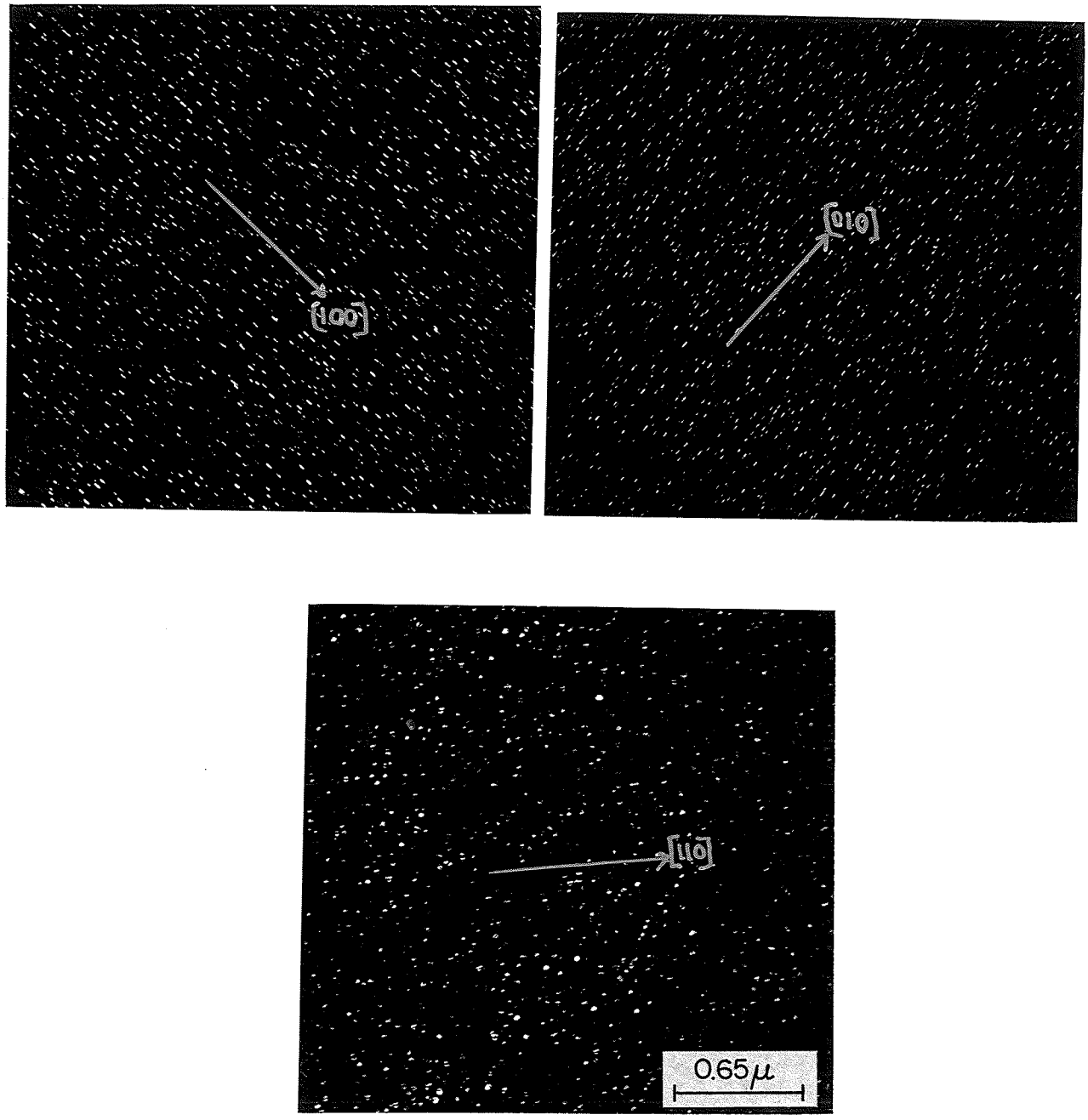

Figure 30. Series of dark field micrographs corresponding to figure 29, imaged with: (a) ($\frac{1}{2}$10) γ", (b) (1$\frac{1}{2}$0) γ" and (c) (110) $\gamma'+\gamma$" reflections.

In addition to these phases the β Ni_3Nb orthorombic phase and very small amounts of NbC were observed at the grain boundary (figure 31). The equilibrium β phase formed through a cellular reaction which could be detected after 10 hours of aging, (figure 32). In nickel base, Nb containing alloys the grain boundary precipitates were identified initially as sheets of NbC phase which then transformed to $M_{23}C_6$ [16]. But in this case the β and NbC phases were identified, which is in agreement with other observations [12]. Around the β particles a precipitate free zone was observed. The γ" particles along side this zone were the same size as those further away from the boundary. Aging for 100 hours or more caused considerable coarsening of the precipitates as seen in figure 33a and b. Figure 34 is a bright field image of a thin foil in a [001] orientation, from a specimen aged for 720 hours at 973 K. The dark fields in figures 35a and b corresponding to the above selected area clearly show the growth of the particles. From these photomicrographs it is estimated that the aspect ratio, ie. the ratio of diameter to thickness, of the the γ" particles increases with time.

Also the PFZ around the β particles grew considerably with time. More needles of the β phase nucleated in the boundaries and grew into the grains (figure 36), which was in agreement with the observations of Raghavan [12] and Kirman et. al. [16].

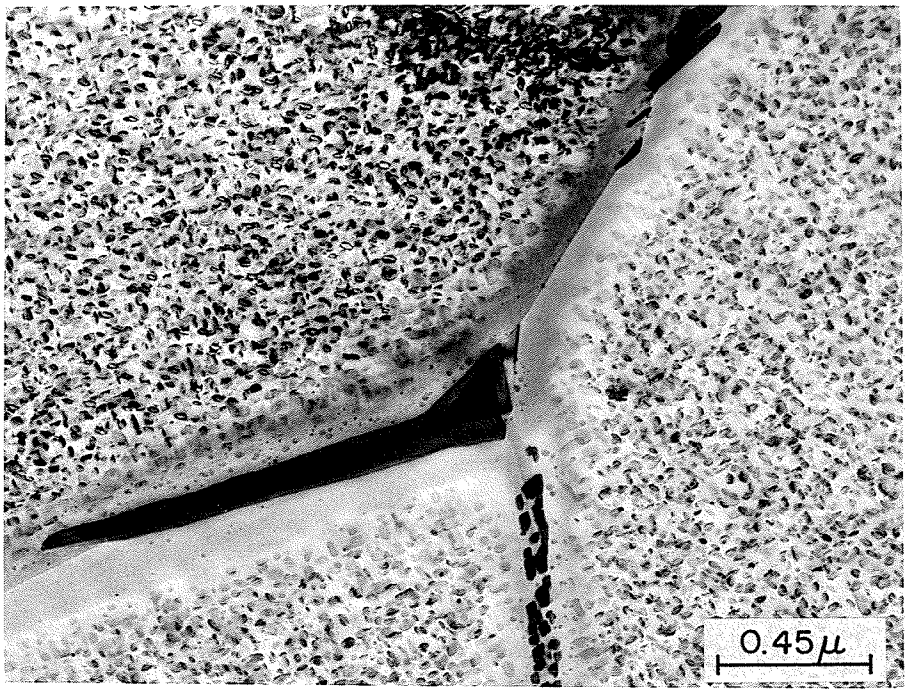

Figure 31. Bright field image showing the precipitate free zone and the β phase on the grain boundaries of a specimen aged for 25 hours at 973 K.

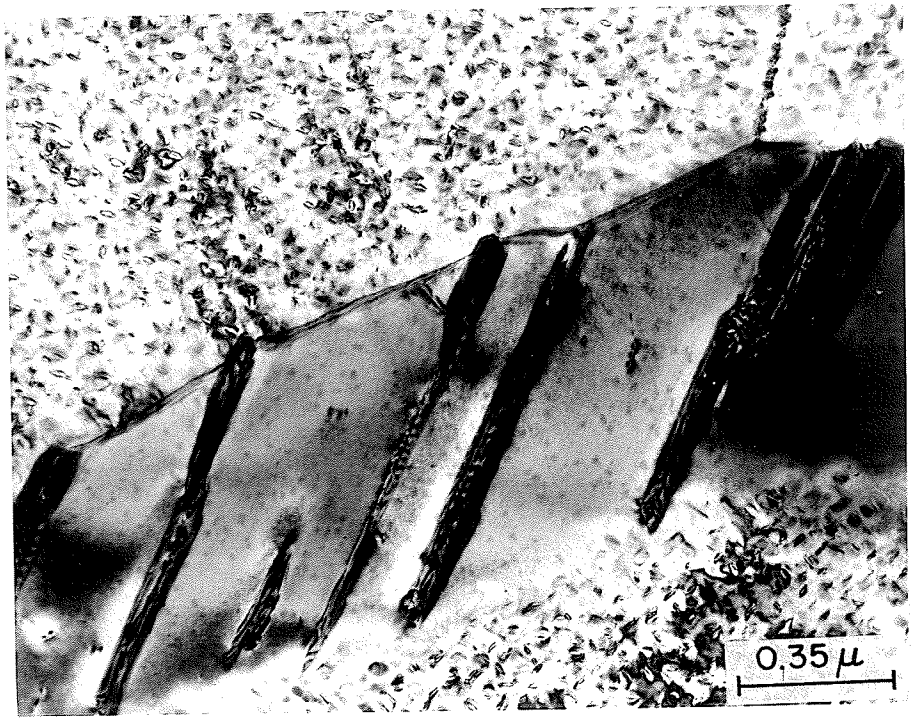

Figure 32. Cellular precipitates at the grain boundary of a specimen aged at 973 K for 10 hours.

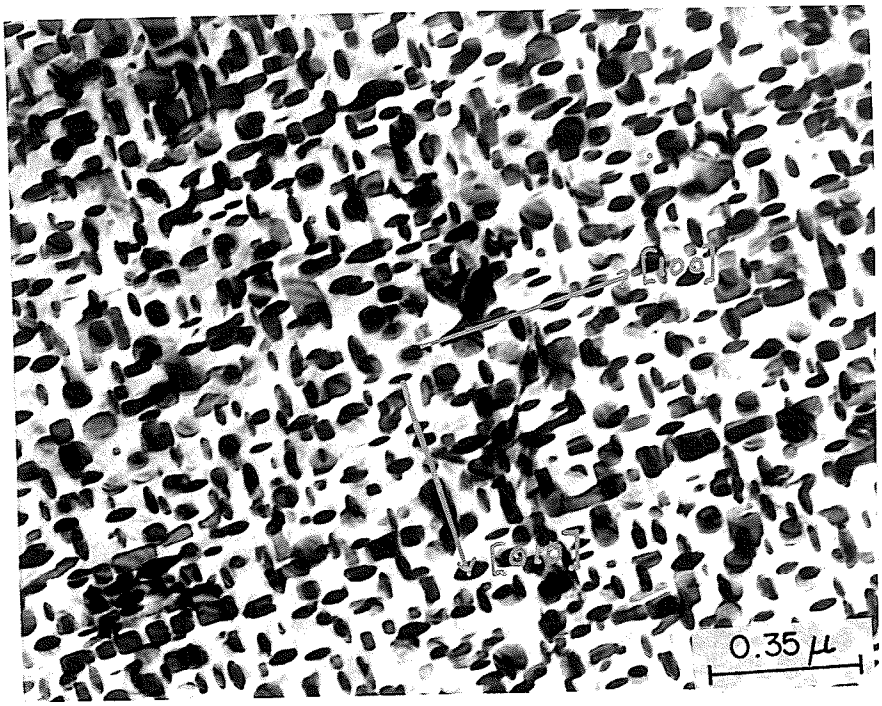

(a)

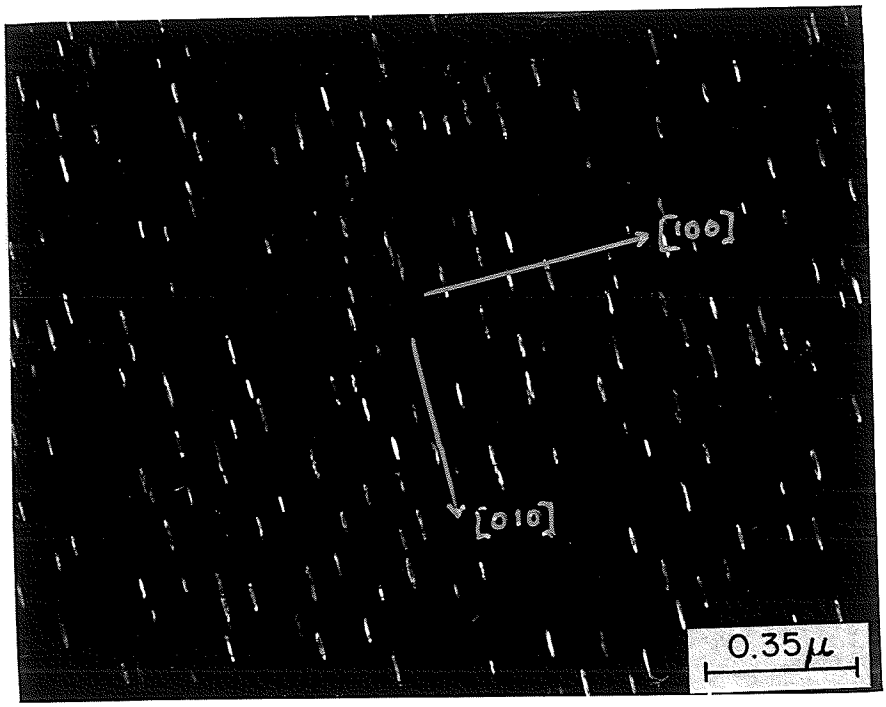

(b)

Figure 33 (a) Bright field micrograph of a specimen aged at 973 K for 100 hours. [100] foil orientation.

(b) dark field image taken with $(1\frac{1}{2}0)$ γ'' reflection.

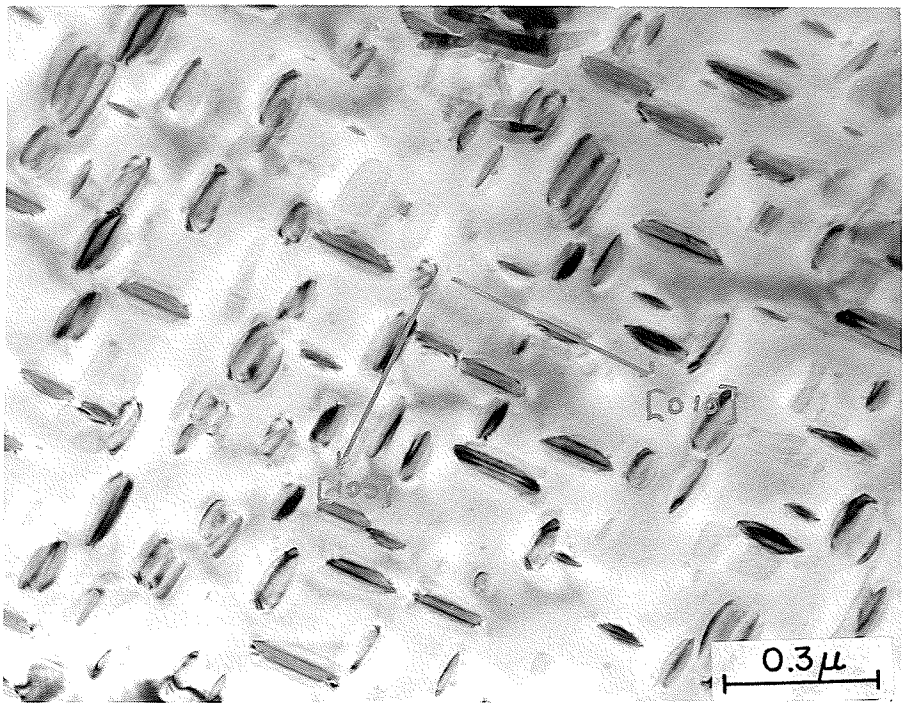

Figure 34. Bright field of specimen aged at 973 K for 720 hours. Shows coarsening of the precipitates.

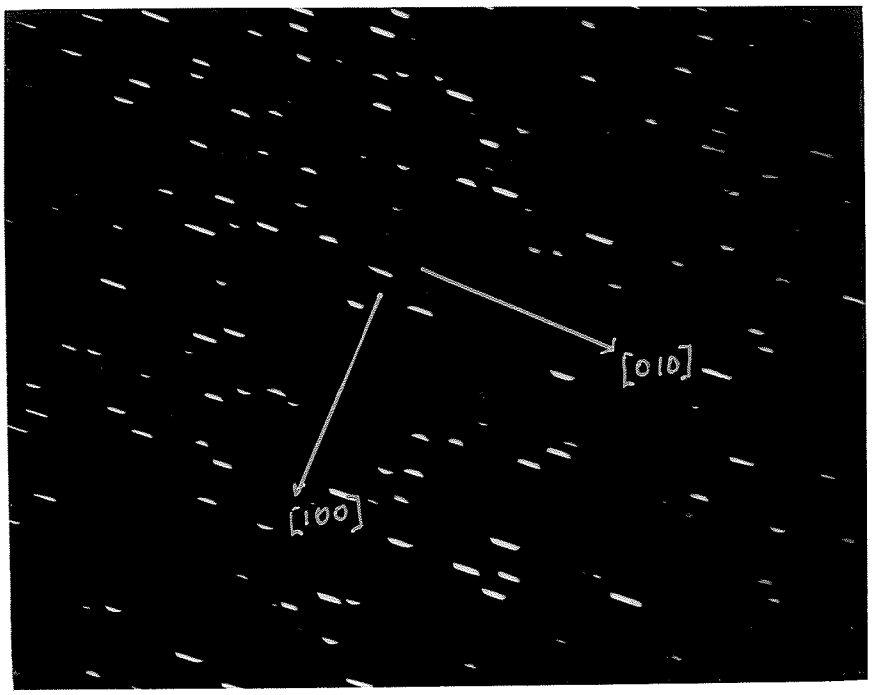

(a)

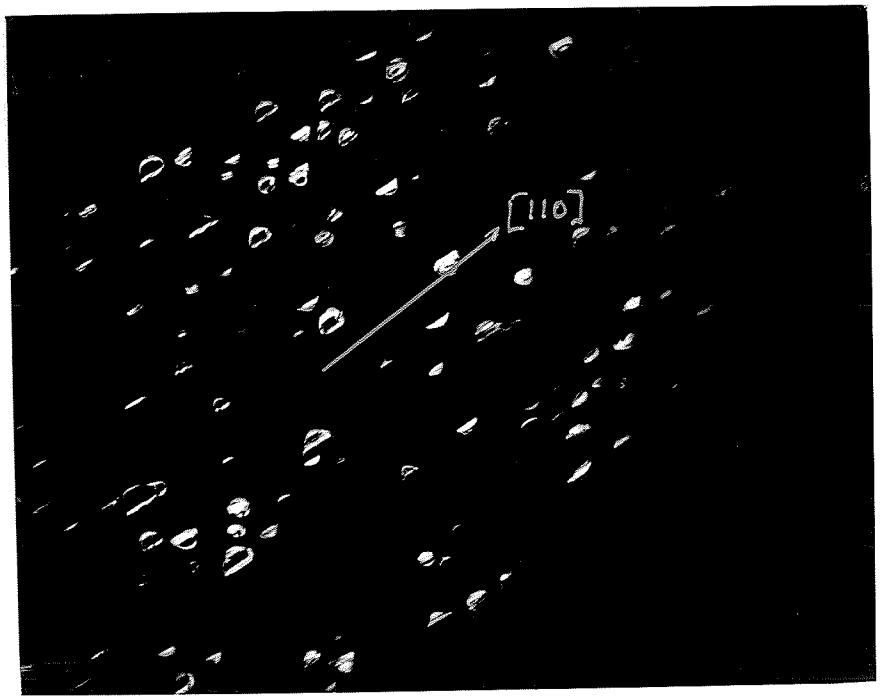

(b)

Figure 35. Series of dark field micrographs of figure 34;
(a) taken with $(1\frac{1}{2}0)$ γ'' reflection,
(b) taken with $(110)(\gamma'+\gamma'')$ reflection.

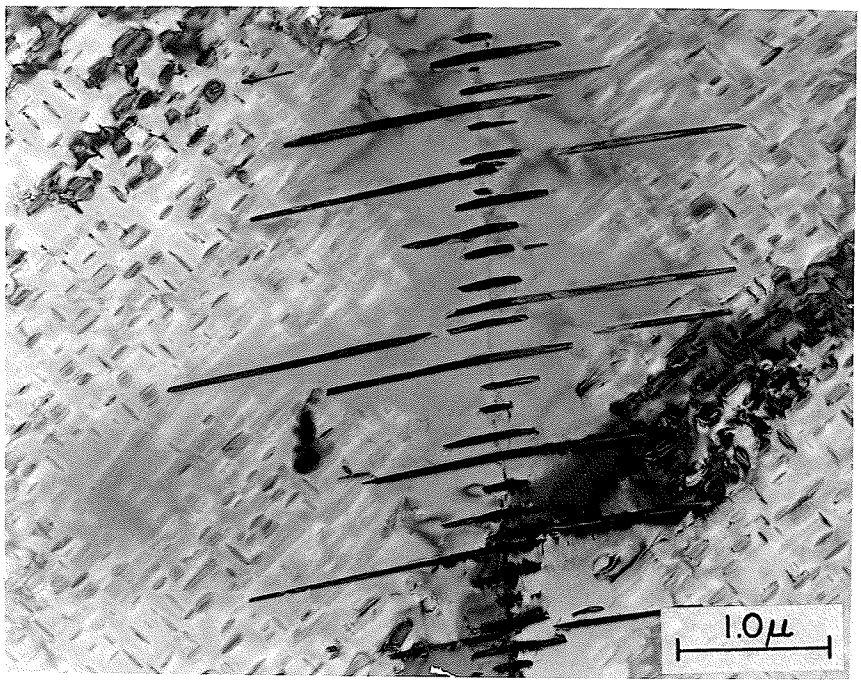

(a)

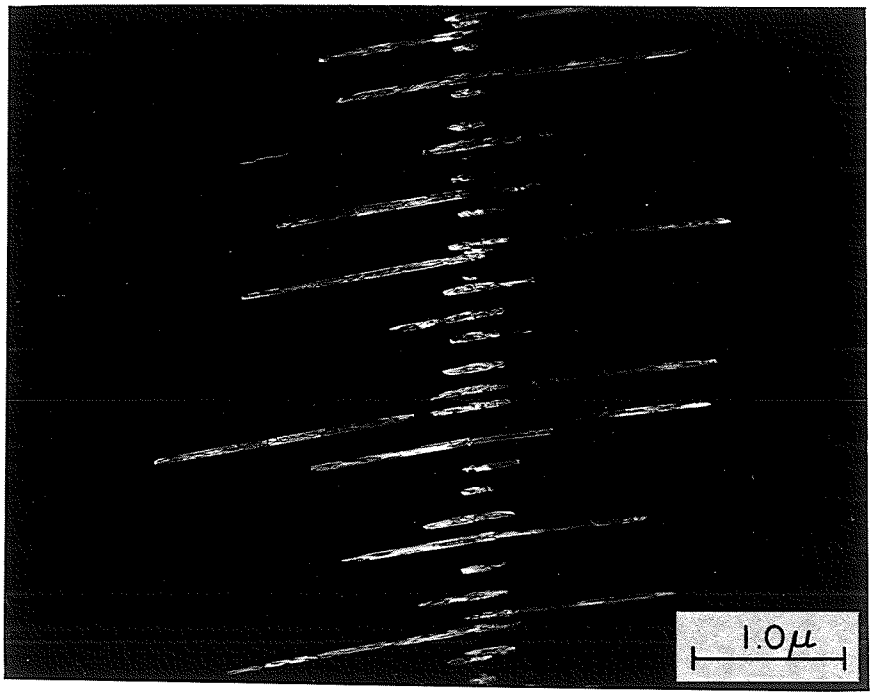

(b)

Figure 36. Transmission electron micrographs of a specimen aged at 973 K for 720 hours, showing needle type β particles growing into the grains; (a) bright field, (b) dark field.

The microstructure, after aging for 720 hours, was characterized by the formation of widmanstatten β platelets.

Bulk specimens were polished and etched in order to be examined under the SEM. Secondary and backscattered electron images were obtained (figure 37) which clearly shows the widmanstatten structure and also suggests that the grain boundary cellular precipitates also transformed to widmanstatten β.

4.4.4 Aging at 1023 and 1073 K.

At 1023 K the precipitation process was expedited. Thus in minutes of aging, γ" particles appeared in the matrix. Figure 38 is a bright field of a specimen aged for 45 hours clearly showing the γ" particles. Adjacent to some of the γ" particles, some γ" precipitates appear, therefore forming a compact morphology as described in detail by Cozar and Pineau [22].

At 1073 K most of the γ" particles were transformed to the equilibrium β phase. The single crystal diffraction pattern of a precipitate extracted by carbon replica technique from a specimen aged for 20 hours at 1073 K and its interpretation are shown in figures 39 and 40.

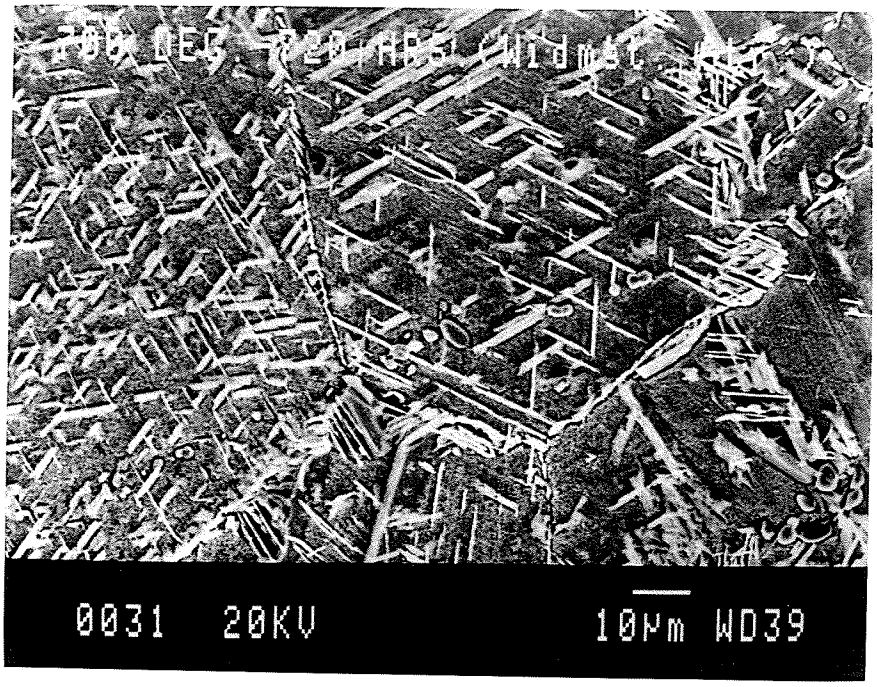

(a)

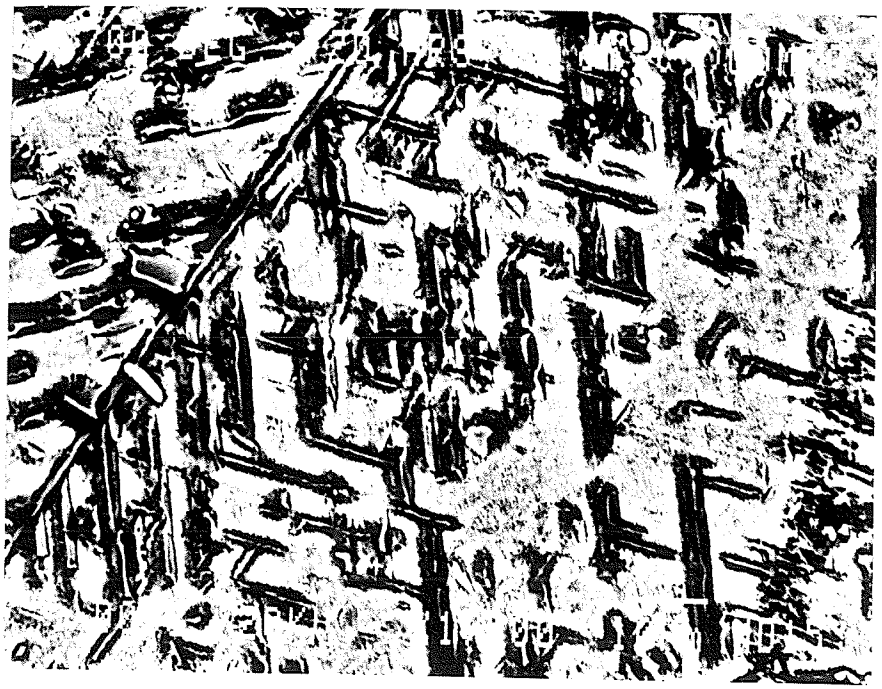

(b)

Figure 37. Microstructure of a specimen aged at 973 K for 720 hours, showing the formation of the Widmanstatten β precipitates; (a) secondary electron, and (b) backscattered electron images.

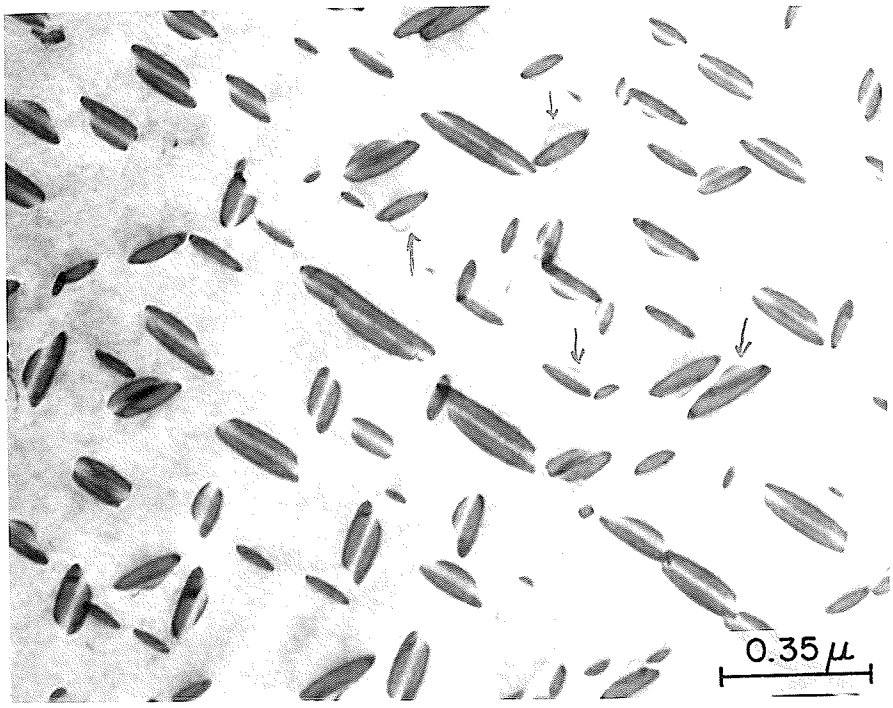

Figure 38. Specimen aged for 45 hours at 1023 K. Bright field image, showing γ" and γ' particles. (Arrows indicate γ' particles.)

(a)

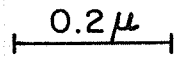

(b)

Figure 39 (a) Single crystal extracted by carbon replica of a specimen aged at 1073 K for 20 hours.

(b) Electron diffraction pattern of the precipitate.

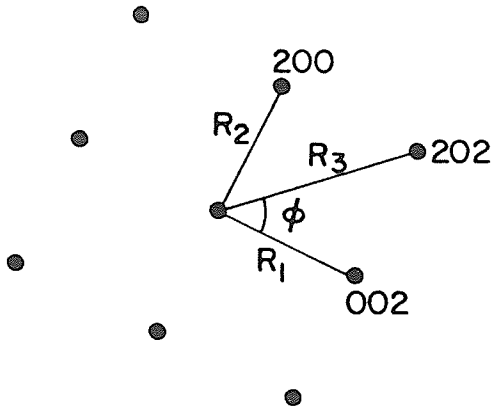

Ratio	Theoretical Values of β phase	Calculated values.
R_3/R_1	1.33	1.339
R_3/R_2	1.50	1.50
R_1/R_2	1.12	1.13
ϕ^0	41.7	41.7

Figure 40. Indexing of the diffraction pattern shown in figure 39b. The particle is identified as β-Ni_3Nb phase.

The lengths of R_1, R_2 and R_3 shown in figure 40 were measured and their corresponding ratio was found to agree closely with the theoretical values of the Ni_3Nb - β phase. Also the angle ϕ, between (202) and (002) was measured and its value was equal to the theoretical value of 41.7^0

4.5 Chemical analysis of γ' and γ'' precipitates.

The precipitates were extracted on carbon replicas and they were placed on carbon coated nylon grids. A chemical microanalysis was conducted on these particles using Energy Dispersive Spectrometry in SEM. The x-rays produced, were picked up and analyzed with a Tracor Northern MCA. The technique employed for analysis has been described in detail in the previous chapter. Over ten different particles were analyzed and the results were averaged.

The γ' particles were extracted from specimens aged at 873 K for 140 and 200 hours and their composition was determined. The results seem to be fairly accurate, ie. the standard deviation is only about 0.1, for ten different microscans. The x-ray spectrum for a γ' particle is shown in figure 41, and its analysis is seen in Table 6. The electron to atom (e/a) ratio was calculated using these results and it was found to be 8.618 for the γ' Ni_3Nb phase.

The chemical analysis of the γ'' particles was not very accurate due to the fact that it was not possible to differentiate between γ' and γ'' in the SEM, since the electron beam spot size in the SEM is too large.

However it was established that the γ'' phase was leaner in iron and richer in nickel content.

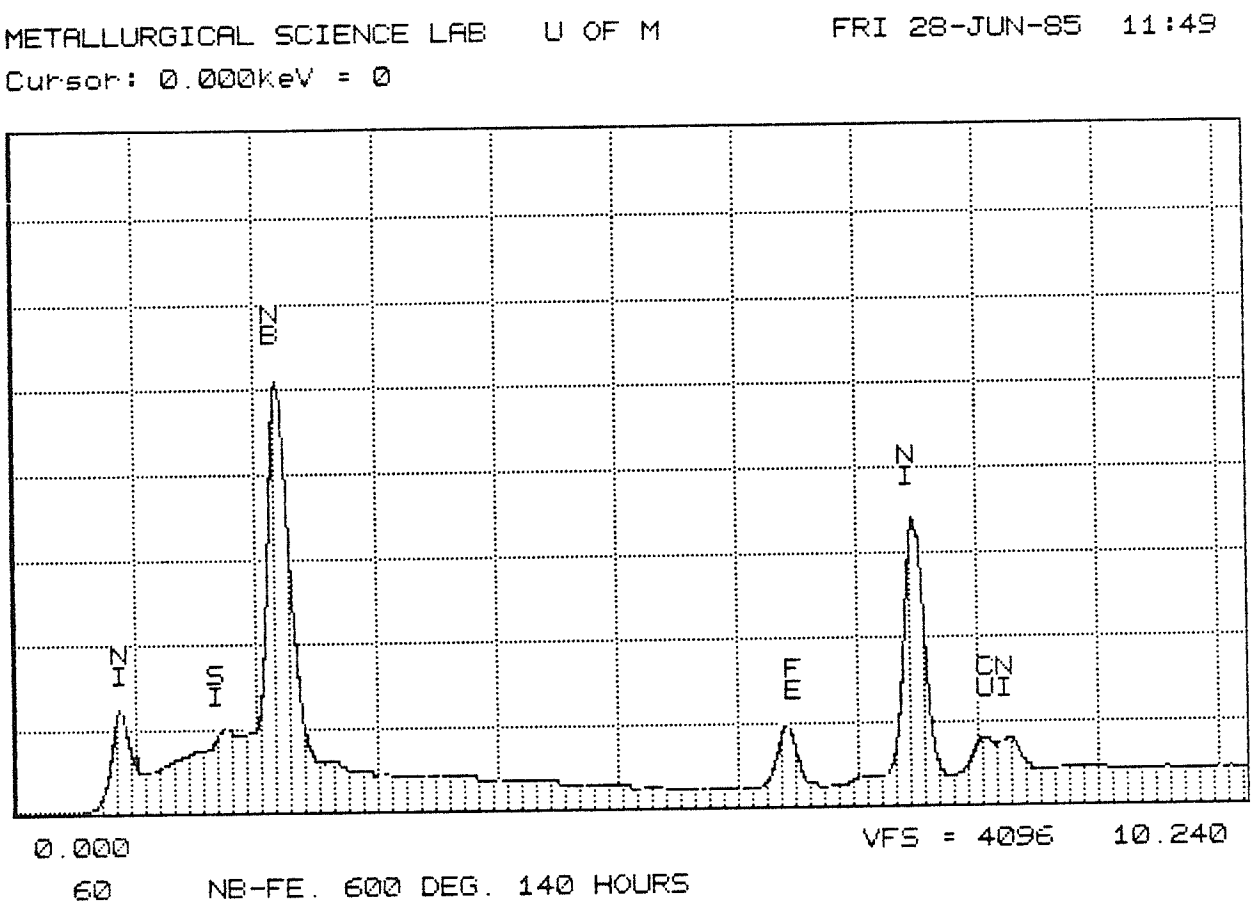

Figure 41. Typical x-ray spectrum of a γ'-$L1_2$-Ni_3Nb particle.

TABLE 6

Analysis of the spectrum shown in figure 41, showing the chemical composition of the γ' Ni_3Nb particles.

REF.S EDS:FEK EDS:NIK EDS:CUK EDS:NBL

ZAF CORRECTION 20.00 KV 40.00 Deg

No. Of Iterations 2

----	K	[Z]	[A]	[F]	[ZAF]	ATOM.%	WT.%	NORM.WT.%
FE-K	0.058	0.982	1.033	0.882	0.896	8.17	5.23	6.75
NI-K	0.400	0.963	1.025	1.000	0.988	58.61	39.57	51.02
CU-K	0.055	1.011	1.017	1.000	1.029	7.82	5.73	7.39
NB-L	0.203	1.053	1.261	0.998	1.328	25.40	27.03	34.85
						Total=	77.56	

* - High Absorbance

Chapter V

DISCUSSION

The results of this investigation show that the precipitation process in the Cu-30Ni-2Nb-4Fe alloy depends on the temperature of aging. Firstly, aging at 873 K produced the γ' $L1_2$ (Ni_3Nb) phase, which was the only strengthening precipitate at this temperature. No discontinuous transformation was observed up to 1500 hours of aging. However, at 973 K the microstructural features of the alloy altered completely. The major strengthening phase here, was the γ'' DO_{22} (Ni_3Nb) phase, coexisting with small amounts of γ'. Other phases such as the equilibrium β (Ni_3Nb) and some NbC also appeared at the grain boundaries. On continued aging the γ'' particles transformed to the stable β phase which grew into the grains, finally to give rise to the widmanstatten structure.

In this chapter the precipitation behaviour of this alloy is discussed in light of the Hume-Rothery theory, the Hagel-Beattie findings and other principles concerning the formation and stability of the γ' and γ'' strengthening phases.

5.1 Precipitation Behaviour.

5.1.1 Solution treated structure.

Transmission electron micrographs of the alloy in the as-quenched condition did not show any definite precipitating phase. The diffraction pattern did not exhibit any super-lattice reflections. However, a modulated structure existed, which indicates initiation of the decomposition of the solid solution. During quenching from the solution treatment temperature (1373 K), the degree of supersaturation increases rapidly, ie. the free energy of the system increases. And since the diffusion distances for nucleation during the early stages are small, the short time available during quenching is not sufficient to supress the formation of new phases. The formation of these nuclei of a second phase with a composition different from the matrix, causes the free energy of the system to decrease. In other words this causes the precipitation process, which can decrease the supersaturation and thus cause a decrease in the free energy of the system to occur.

Therefore, the formation of these discrete ordered particles formed at this stage, suggests that the decomposition of the supersaturated solution occurs by homogeneous nucleation.

5.1.2 Variation in the lattice parameter of the matrix.

The lattice constant of the solution treated supersaturated solid solution was found to be 3.590 Å. On aging at 873 K, the lattice parameter showed a decrease during the initial stages of aging and then remained constant up to 140 hours of aging. Even at higher temperatures, ie. 973 and 1023 K, a slight decrease in the lattice parameter was noticeable (ie. 3.587 Å)

In the as quenched solid solution the total number of solute atoms and their sites will govern the lattice parameter of the matrix. But during aging other factors come into play and influence the lattice parameter changes. Since the lattice constant of both the γ' and γ'' is slightly larger than the $a\gamma$ (Table 2), these particles will be restrained from expanding by the elastic forces in the matrix. Baker et. al. [44] have shown that hydrostatic forces arise during the growth of a coherent precipitate. In addition to all this, the γ' and γ'' precipitates may cause a depletion of solute atoms, ie. niobium and iron, in the matrix which would explain the small decrease in $a\gamma$.

However, this decrease in $a\gamma$ is so small that it could easily be attributed to a combination of all the above mentioned factors.

5.1.3 Shape of the γ' particles.

The γ' particles nucleated homogeneously in the matrix on aging at 873 K. The shape of these particles was perfectly spherical (figure 15b). Progressively, with increasing aging time, some of the precipitates seemed to transform to a cuboidal shape. On aging at 873 K, for 1000 hours, the shape of most of them was clearly cubical with rounded edges (figure 42).

Hagel and Beattie [30] have suggested that when the lattice misfit between γ' and γ is less than 0.5 pct, the γ' particles develop a spherical shape, while when the misfit is in the range of 0.5 - 1.0 pct, cuboids are formed. However, our experimental results show that the γ' particles developed a cuboidal shape even when the γ/γ' value was less than 0.5 %. Therefore, the Hagel and Beattie observation is not applicable to the present system.

Others [45] have shown that the γ' particles are spherical when small but become cuboidal upon increasing in size. This is in agreement with the present findings, as the shape of most of the γ' precipitates changed from spherical (when small) to cuboidal as they grew; it is likely that 1500 hours is not sufficient for all of them to change their shape to cuboidal.

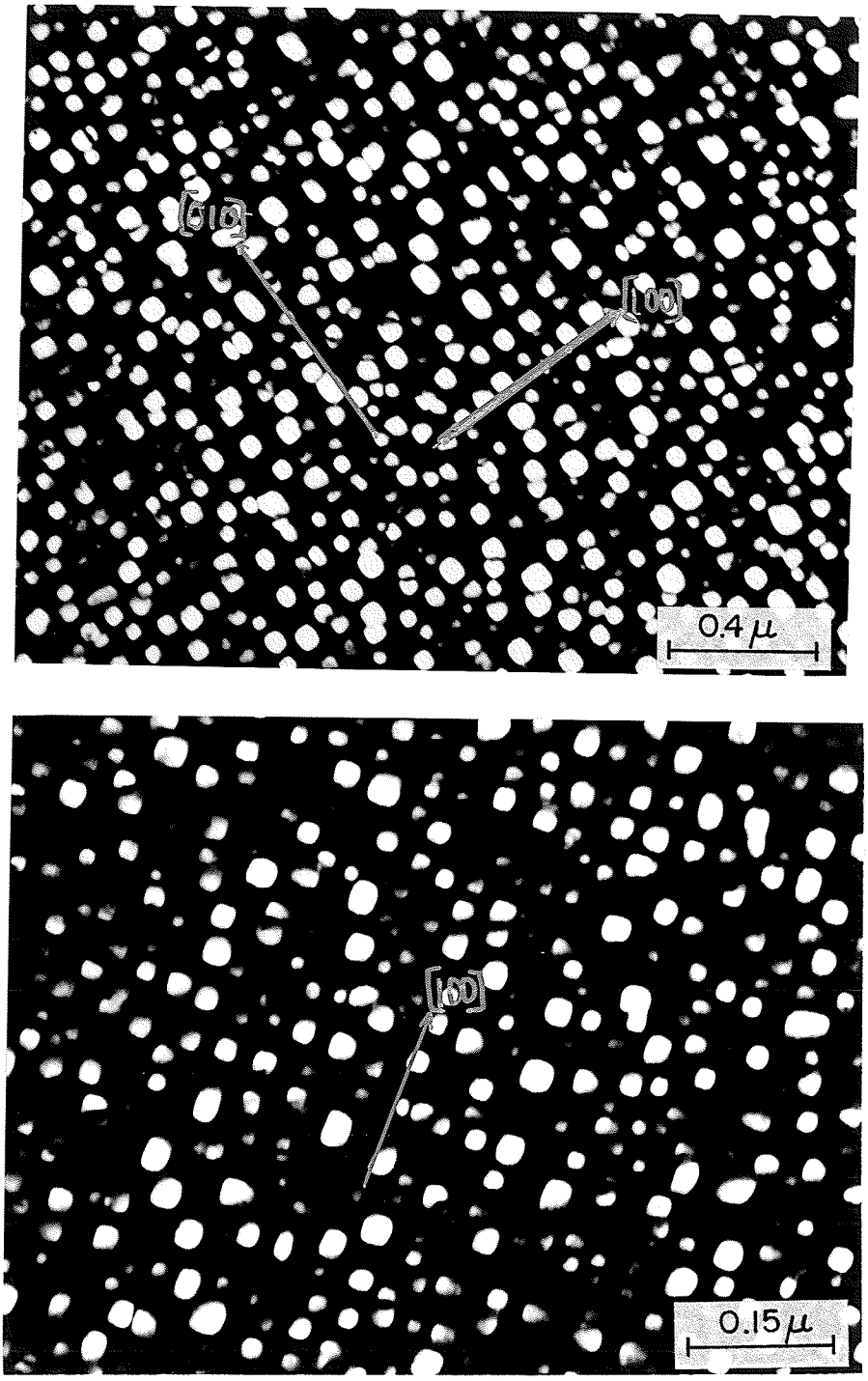

Figure 42. Dark field micrographs of a specimen aged for 1200 hours at 873 K. The quasi-cubical morphology of the γ' particles is evident.

5.1.4 Lattice mismatch between γ/γ'

It was mentioned in section 2, that according to Hagel and Beattie [30], coherent precipitation of γ' type phases will be inhibited when the lattice misfit between γ/γ' exceeds 1.0 pct.

Quist's work [25] verified that the appearance of γ' and γ'' precipitates on the Ni-Nb system followed this requirement for interfacial matching.

The lattice parameter of the γ' phase in the present investigation was found by electron diffraction to be approximately the same as that of the matrix, ie. 3.589 Å at 873 K. However, at 973 K, where γ' coexisted with the γ' precipitates, the $a\gamma''$ was determined to be 3.620 Å. Therefore in both cases the lattice mismatch between γ/γ' is less than 1.0 pct, which indicates that the Hagel-Beattie suggestion is applicable to the present system.

5.1.5 Strength characteristics.

The increase in hardness at 873 K is clearly due to precipitation of the γ' phase. There is also little doubt that the hardening at 973 K is brought about by the γ'' phase. The peak hardness obtained at 973 K was higher than the one at 873 K.

In the same manner the tensile results show that on aging at 873 K, the increase in YS and UTS is less sensitive to aging time. But on aging at 973 K, the YS of the alloy increased by 250 pct over the solution treated condition and maximum strength is obtained in relatively short aging times. This behaviour is indicative of a change in the sequence of phase transformations between 873 and 973 K, ie. γ' to γ'', which is consistent with the x-ray and electron microscopy results.

However, this is contrary to the normal behaviour, ie. the increase in hardness at the higher temperature of aging is less than that observed at the lower temperature. This may be attributed to the fact that the degree of supersaturation, and the volume fraction of the precipitates is greater at the lower temperature of aging, than that present at the higher temperature.

Therefore, the observed results may be attributed to the degree of coherency, which in turn must be a significant factor in the strength of this alloy.

Figures 9 and 23 indicate that the coherency strain associated with the γ'' bct particles was considerably greater than that for γ'. This may well be because of a significantly larger value of misfit in γ/γ'' (0.0281), as compared to only 0.003 for γ/γ'.

Kirman [15], pointed out that in Nb containing, iron-nickel base alloys, overaging is due to the formation of the β phase. Later work [12] on a Nb containing cupronickel is in agreement with this observation. The present investigation indicates softening of the alloy only after about 70 hours at 973 K. The equilibrium β precipitates appeared in the boundary long before that, but nearly 100 hours of aging was needed to produce significant amounts of β phase, which grew into the grains. In addition to this, aging at 1073 K proceeded very rapidly and was accompanied by rapid β-Ni_3Nb formation.

Thus, in support of the earlier findings, it is suggested that the primary loss of hardness at 973 K was due to the transformation of γ" particles to orthorombic β-Ni_3Nb. There was no evidence that overaging of the alloy was related to coarsening of the γ" particles.

5.1.6 Precipitate free zone and grain boundary precipitates.

The results of the present investigation indicate that the PFZ was solute depleted since no preferential coarsening of the γ' (at 873 K) or the γ" (at 973 K) particles at the PFZ boundary was observed (figures 22 and 23). This differs from Ni base alloys containing Nb which, according to Kirman and Warrington [16] may exhibit PFZ due to solute or va-

cancy depletion. However, an investigation of a Cu-30Ni-Nb alloy [12] has shown that the PFZ in the copper base alloy was solute depleted. More scientific evidence on this was provided by Raghavan [46], who conducted EDS microanalysis of precipitate free zones in Al-Zn-Mg and Cu-Ni-Nb alloys. Solute concentration profiles across a grain boundary in the as quenched and aged samples were mapped by conducting microanalysis on five locations symmetrically accross the grain boundary. Figure 43 shows the Nb concentration profiles in the as quenched and aged sample of the Cu-Ni-Nb alloy. It is seen that in the as quenched sample the Nb concentration was fairly uniform across the grain boundary. In the aged sample, the Nb concentration showed a rapid decline at the PFZ boundary and it was negligibly small at the grain boundary. These observations confirm the suggestion that the PFZ was solute depleted. Figure 43 shows that the Nb concentration within the grains ($C\gamma/\gamma"$) is higher than at that of the PFZ ($C\gamma/\beta$).

The PFZ formation of the alloy studied in this investigation can be explained with these observations and a schematic diagram is shown in figure 44. During the early stages of aging, the β phase nucleates at the boundary as $\gamma"$ particles form homogeneously within the grain. It was found that $C\gamma/\beta < C\gamma/\gamma"$ (figure 43), which means that nucleation of the β phase at the boundary depletes Nb. Thus a zone, on either side of the boundary will have a Nb concentration which is

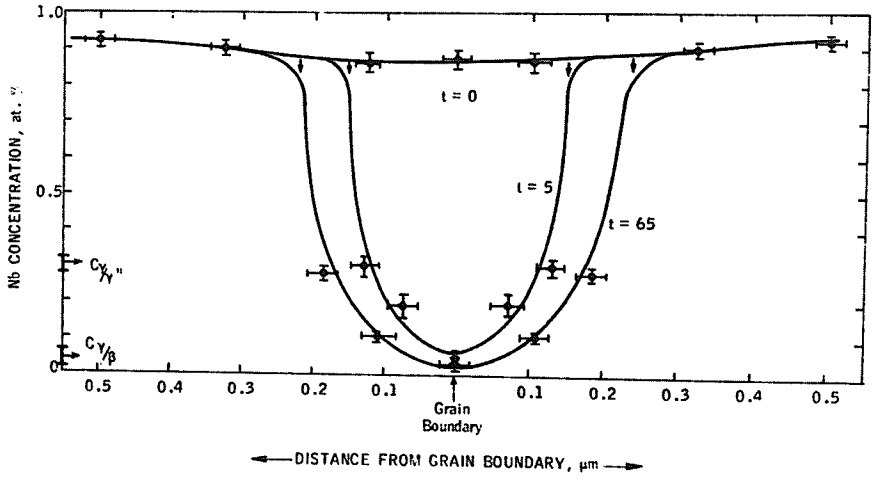

Figure 43. Nb concentration profiles across the PFZ of a Cu-30 % Ni-Nb alloy, in the as quenched (t=0), and aged conditions (t=5, 65 hours at 973 K) [46].

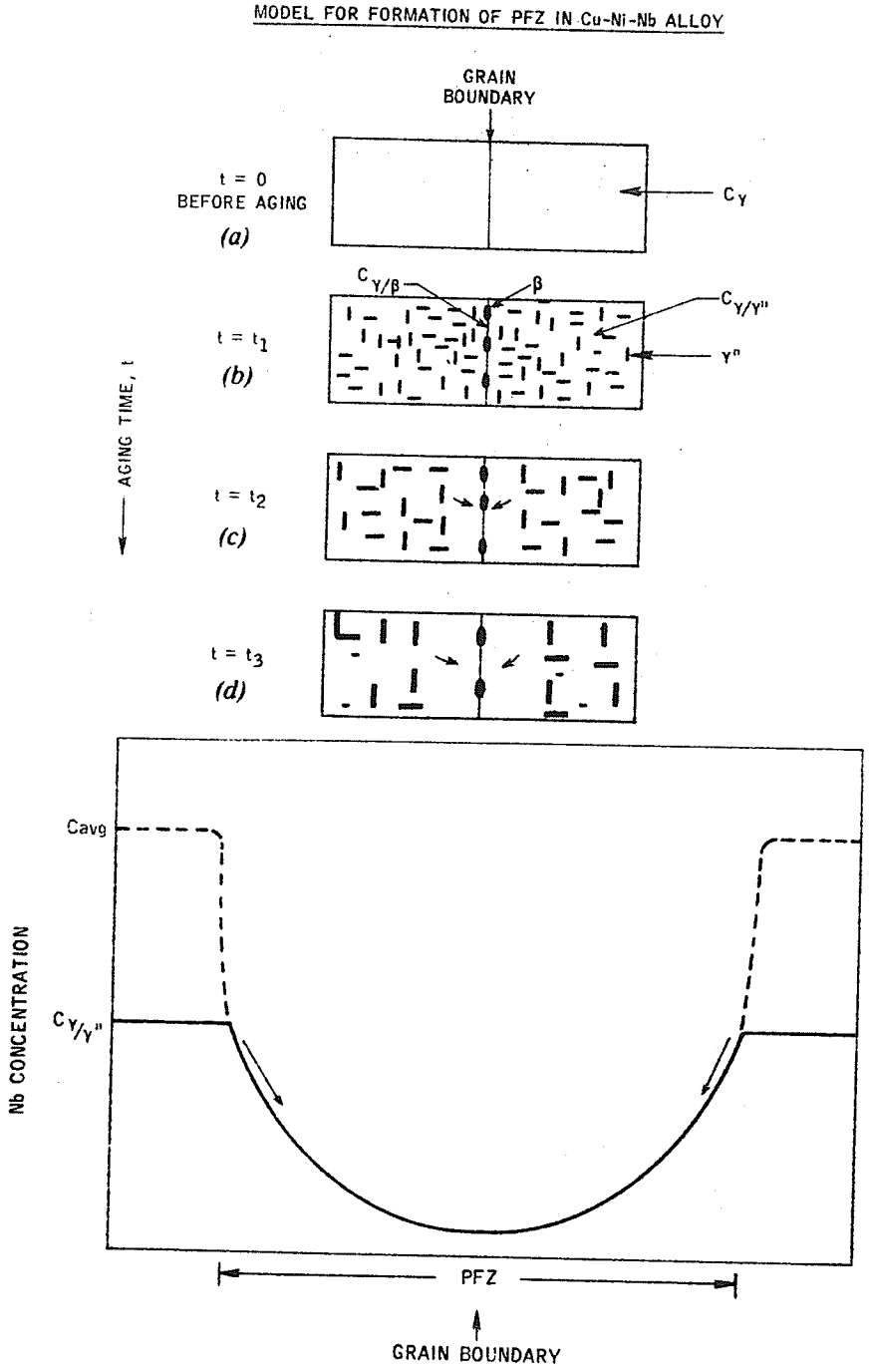

Figure 44. Schematic representation of the formation of PFZ in Cu-Ni-Nb alloys. The matrix solute concentration across the boundary is shown below. The arrows indicate the diffusion of solute [46].

between $C\gamma/\gamma''$ and $C\gamma/\beta$. So the γ'' precipitates do not form in this zone but form within the grains, and the Nb concentration of the matrix at t=0 (solution treated) drops to a value of $C\gamma/\gamma''$. Since $C\gamma/\gamma'' > C\gamma/\beta$, a diffusion gradient is formed while γ'' particles dissolve and Nb diffuses towards the grain boundary to form the β phase. Since the diffusing Nb atoms move towards the boundary (figure 44), the γ'' particles at the PFZ do not coarsen but the PFZ widens with time, as was observed in the present investigation.

5.2 Formation and stability of the γ' and γ'' phases.

5.2.1 Crystallographic considerations.

Quist et. al. [25] argued that of the sixty-four $L1_2$ compounds reported in binary systems, none was found to form in systems containing fcc and bcc elements unless the bcc component has an hcp or fcc allotrope. The influence of iron on the formation of the $L1_2\gamma'$ phase in the Cu-Ni-Nb alloy may also be understood in terms of such crystallographic considerations. Copper and Nickel are both fcc elements and they form a fcc substitutional solid solution. Iron also exhibits the fcc crystal structure (above 0.65 Tm) and in binary systems with nickel it forms $L1_2$ compounds [25]. Thus additions of iron could promote the formation of a γ' $L1_2$ phase which was the case in the present investigation at 873 K.

Conversely, aging at 973 K was found to promote the formation of a γ" phase. The most probable explanation for this behavior may be due to the different solubility of Fe at 873 and 973 K. With increasing temperature, ie. 973 and 1023 K the solubility of iron will increase close to the value of the solubility limit. It has been suggested [25] that the concentration of iron in the matrix and the different temperatures at which the two phases (γ' and γ") appeared, would determine whether iron exerts influence as a fcc or bcc. We may also suggest that the enhanced solubility of iron in the matrix at 973 K would alter the ratio of the partitioning elements, ie. substitution of iron for nickel and niobium, in γ' and γ", and thereby affect the degree of misfit between matrix and precipitate and also the e/a ratio which is an important criterion for the formation of these compounds.

This explanation is admittedly speculative but is plausible.

5.2.2 The e/a ratio.

The changes in relative stabilities of phases may be evaluated in terms of a model based on the free electron concentration. The e/a ratio, ie. the total number of electrons outside the inert gas shell per atom, is the control-

ling factor in predicting the stability of the A_3B type compounds [26,36].

In Ni-Nb-Fe alloy systems, Quist et. al. [25] discussed the matrix electronic factors which could promote the formation of either γ' or γ'' phase. Sinha [27,28], and later work by Cozar and Pineau [34] on Fe-Ni-Co-Ta alloys showed that the γ'' phase is stabilized when its e/a > 8.65, and the γ' phase is stabilized when its e/a < 8.65. The Cu-Ni-Nb system has been examined by Raghavan [33], who correlated the e/a ratio to the formation of the γ' and γ'' phases. In this alloy the γ'' DO_{22} precipitated, as expected. However, in the presence of aluminum in the same system the microstructural characteristics changed, since aluminum can substitute for niobium in Ni_3Nb and therefore reduce its e/a ratio, as the corresponding ratio is only 3 for aluminum, as compared to 5 for niobium. So when the percentage of aluminum was low, γ'' was stabilized, but with increase in the percentage of aluminum, the e/a ratio was further reduced and γ' was stabilized.

Thus the e/a ratio for the γ' and γ'' particles is affected by the substitution of the alloying elements. It is very important whether substitution occurs for the A or for the B atom in the A_3B structure, because of the differences in the e/a ratios of nickel (A atom) and niobium (B atom), ie. e/a for nickel = 9.0, while e/a for niobium = 5.0. Investiga-

tors agree that aluminum occupies the B position of $L1_2$ type compounds [19,25]. But the influence of iron as a substituting element in a copper base alloy is not clearly understood. The atomic radius of iron is 1.275 Å, which is slightly larger than that of nickel (1.243 Å), but considerably smaller than the radius of niobium (1.43 Å). Nickel and iron are similar in that both are group VII elements of the fourth period, but iron and niobium have the same crystal structure, ie. iron below 911 ^{0}C is bcc. However, both iron and niobium form similar $L1_2$ compounds (Ni_3Nb and Ni_3Fe) when alloyed with nickel. Thus, we can suggest that iron may substitute for both nickel and niobium.

The results of the microanalysis of the γ' $L1_2$ particles at 873 K indicate that approximately 8 atomic pct of iron substitutes for nickel thus decreasing the e/a ratio to 8.618, which is below the 8.65 value required to stabilize the $L1_2$ phase. The chemical composition determined for the DO_{22} $\gamma"$ phase seems to suggest that only 2 atomic pct of iron substituted for niobium, but no iron substituted for nickel. This would increase the e/a ratio of the Ni_3Nb compound to about 8.9 which is in harmony with the above theories.

The results of this investigation clearly demonstrate that the e/a ratio is a powerful tool in predicting the stability of the $\gamma'(L1_2)$ and $\gamma"(DO_{22})$ phases. However this

does not explain why the e/a ratio increased at 973 K, therefore stabilizing the γ" phase. However, it may be suggested that the enhanced solubility of iron in the matrix at the higher temperatures (973 or 1023 K) resulted in precipitates lean in iron, while at lower temperatures the decreased solubility of iron in the matrix produced the γ' precipitate which was richer in iron. This seems to agree with the results of the microanalysis which showed that the amount of iron present in the γ' particles was higher than the iron present in the γ" particles.

5.3 Interaction between γ' and γ".

The examination of the unit cells of γ' and γ" illustrated in figure 45, shows the similarity between the fcc ($L1_2$) and the bct (DO_{22}) phases based on the composition $Ni_3(Nb,Fe)$. Except for the slight distortion along the cγ" axis, these two phases represent ordered variations of the fcc lattice. In the $L1_2$ structure, Nb and some Fe atoms are located at the cube corners, while in the DO_{22} phase, these atoms occupy the centre and the corners of a cell formed by placing two fcc cells one upon the other.

It seems that the transformation from γ' to γ" or γ" to γ' is a relatively easy process, since it only needs to rearrange only a portion of the atoms inside the precipitate.

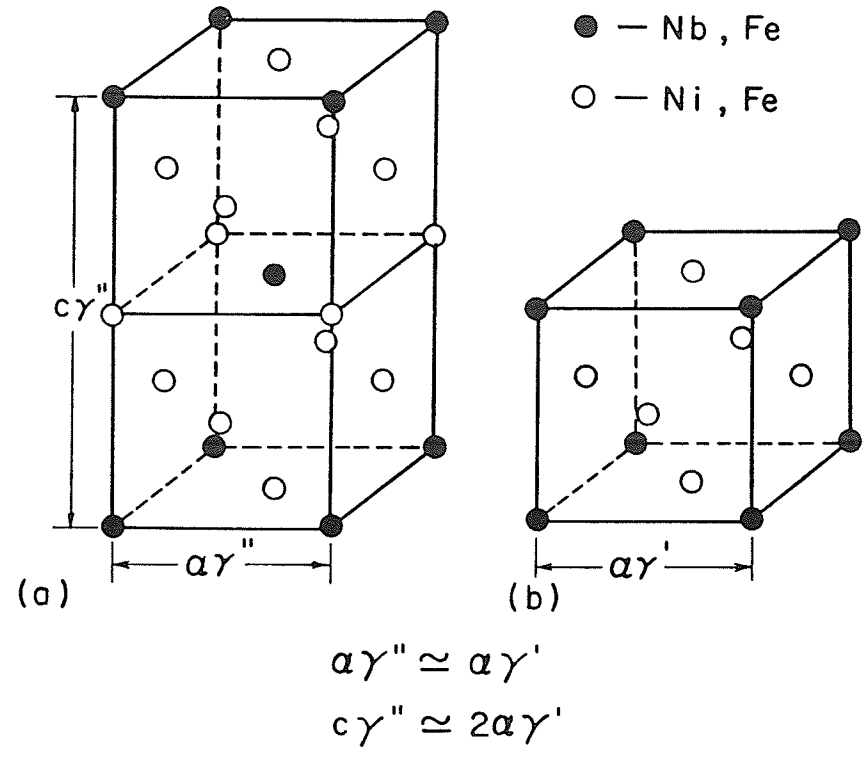

Figure 45. Unit cells showing ordering of (a) bct, (DO_{22}), γ" and (b) fcc, ($L1_2$) γ'. Both structures are ordered variations of the fcc crystal lattice.

So the possibility of stacking (001) γ" planes over one of the three {001} γ' planes without introducing a stacking fault, does exist. Moreover, the γ' lattice parameter is between those of the γ matrix and the γ" phase (figure 45).

It was reported [22] in Inconel 718 alloy that γ' particles had all their six faces coated with a shell of γ" (figure 48). They refered to this kind of morphology as compact.

In the present study many γ' and γ" particles were seen in contact at 973 K (figure 47) and 1023 K. Strangely enough this kind of morphology was observed only during overaging or at higher temperatures, ie. 1023 K. Thus, we may say that the initiation of the γ' and γ" interaction is related to the size of the γ' and γ" particles.

Cozar et. al. [22] showed that the compact morphology could only be observed if the γ' particles had reached a minimum critical size (Lc). A schematic diagram shown in figure 49 demonstrates the initiation and occurrence of the compact morphology. Consider a small γ' particle with a γ" particle nucleated on it as shown in figure 49a. The γ" precipitate forms preferentially on one of the six faces of γ' when an increase in dimension L takes place, the γ" particle overlaps the γ', (figure 49b). Around this γ" particle the Niobium concentration is lowered, ie. the diffusion zone shown in figure 49b (shaded area). The lower Niobium

concentration at A or B decreases the probability of γ" precipitation in this region. The resulting microstructures are, those observed when small particles are formed (figure 49c). But at higher temperatures, larger isolated γ' precipitates can be formed, and precipitation can occur more easily on the six faces of the cube-shaped γ' particles as seen in figures 49e and f.

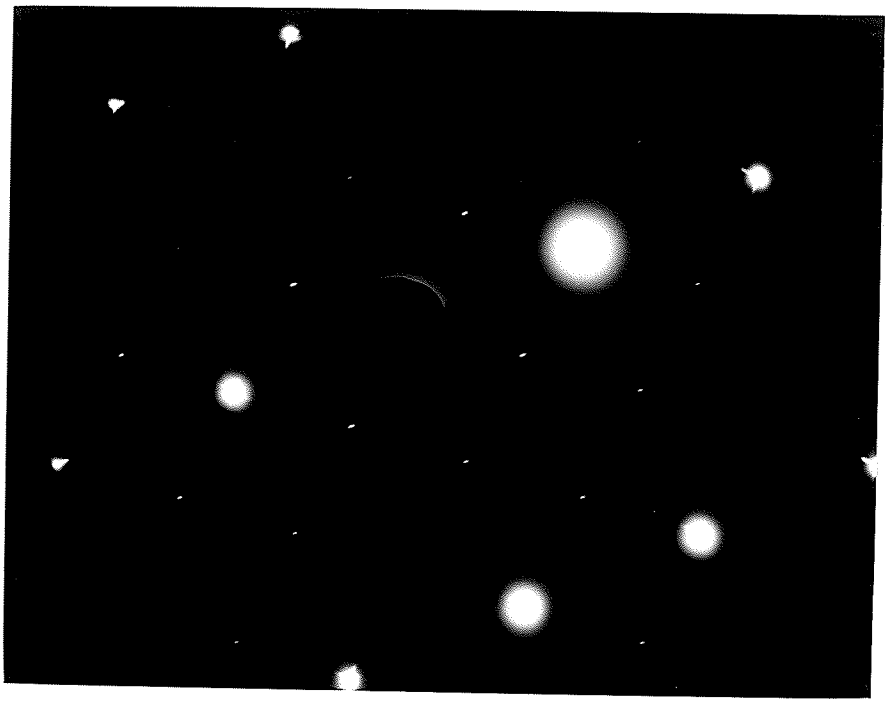

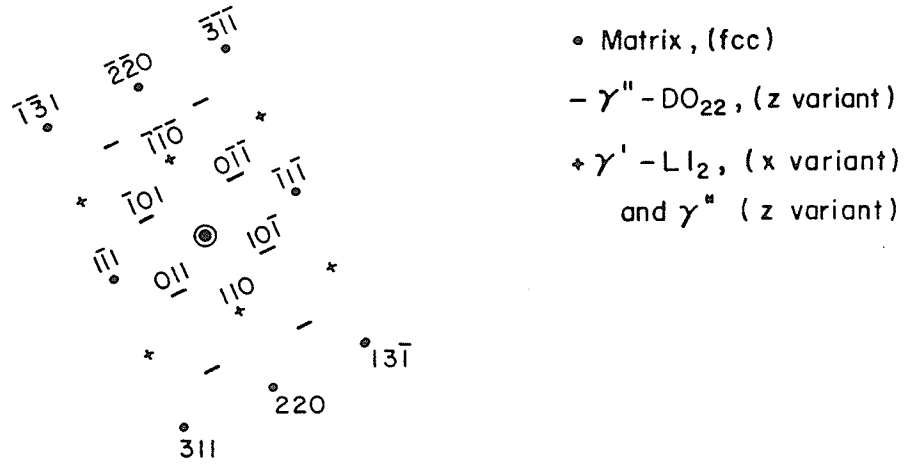

Figure 46. Diffraction pattern of a specimen aged at 973 K for 600 hours. B = [112]

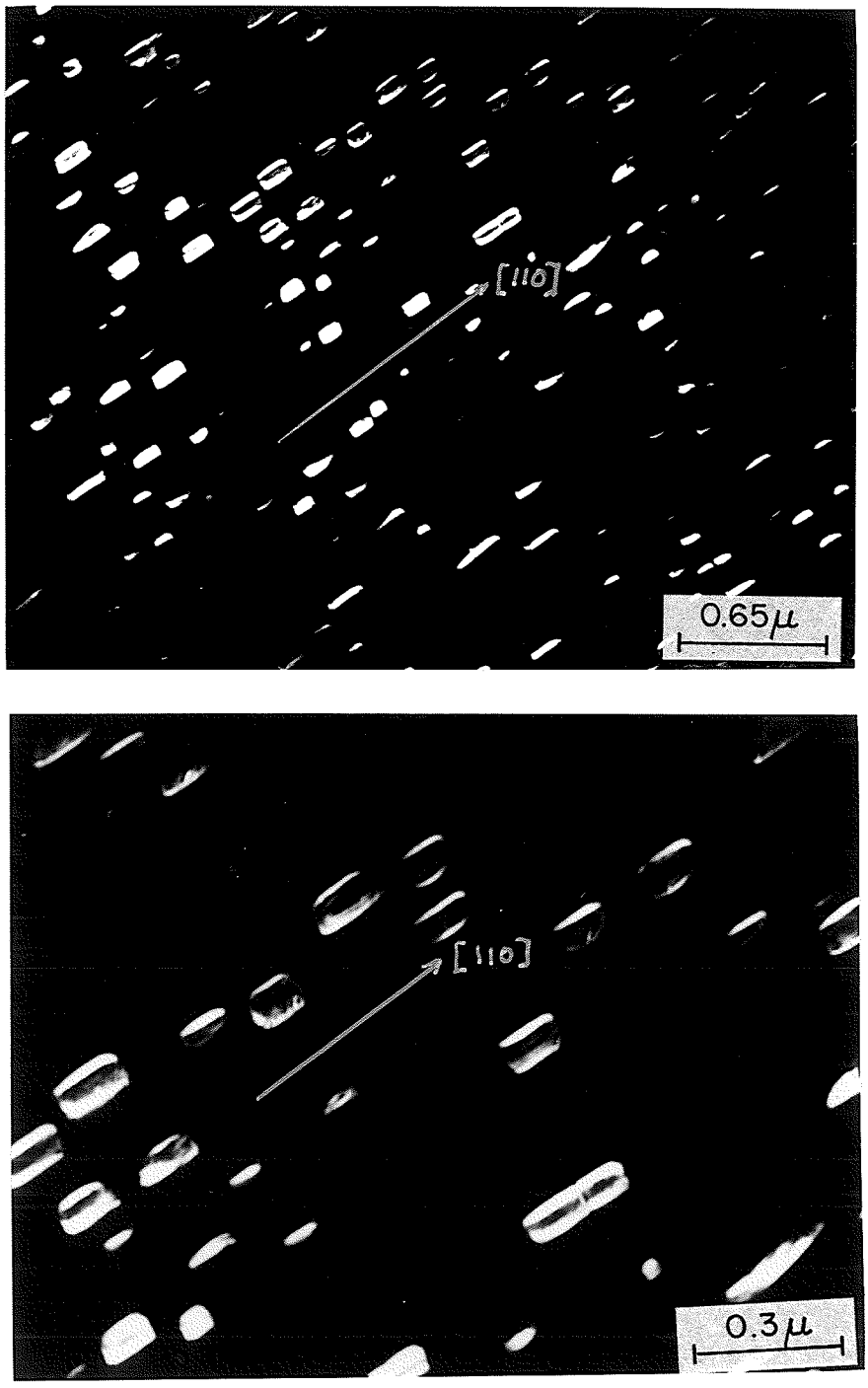

Figure 47. Dark field micrographs imaged with (110) reflection of the DP shown in figure 46. Both γ' and γ'' are visible.

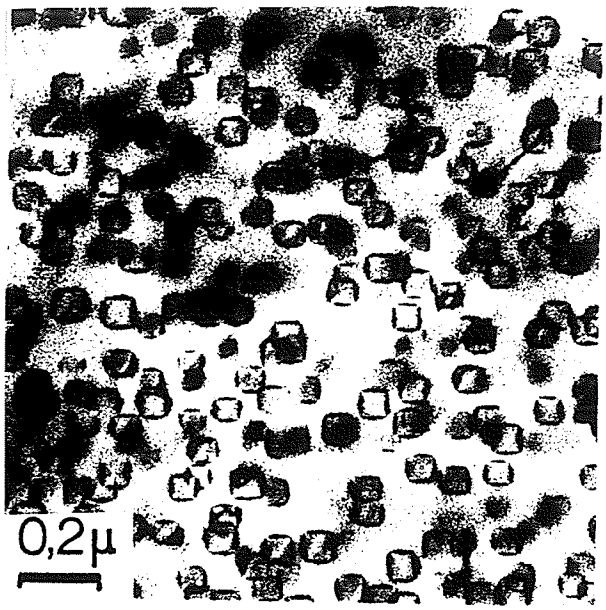

Figure 48. Microstructure of an Inconel alloy aged at 750°C for 524 hours. The interaction between γ' and γ'' is seen [22].

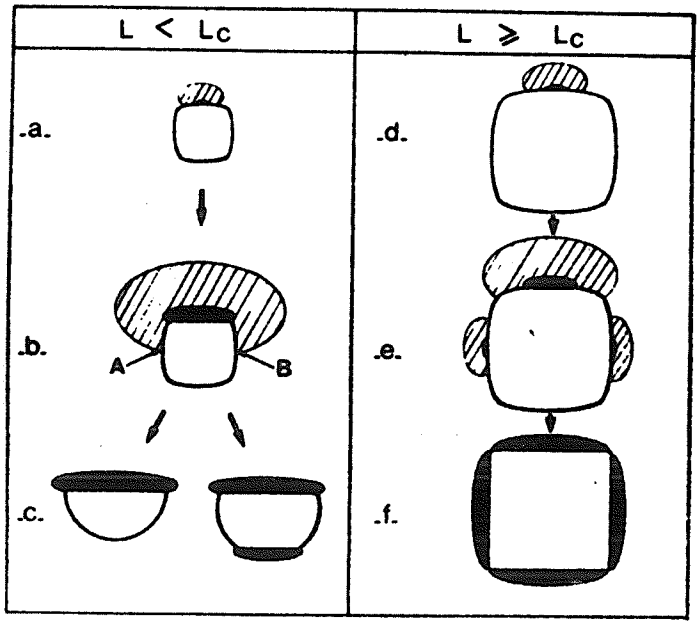

Figure 49. A schematic representation depicting the initiation of compact morphology [22].

Chapter VI

CONCLUSIONS

6.1 The present investigation has demonstrated that age strengthening in the Cu-30Ni-2Nb-4Fe alloy on aging at 873 K was the result of the precipitation of the ordered fcc-γ'-$L1_2$-Ni_3Nb phase which forms on {100} matrix planes. On aging at 973 K the main strengthening phase was the ordered bct γ'' phase which forms coherently with a disc-shaped morphology.

6.2 The change in γ' shape ie. spherical during the early stages turning to cuboidal on prolonged aging, is due to particle size effect alone and not due to γ/γ' lattice mismatch effect.

6.3 Equilibrium β phase formed through a grain boundary cellular reaction on aging at 973 K. On prolonged aging at the same temperature the γ'' transformed to the β(orthorombic) phase which later gave rise to the Widmanstatten structure.

6.4 The loss of strength on aging at 973 K was attributed to the formation of the equilibrium β phase and not due to γ'' particle coarsening.

6.5 The grain boundary precipitation during aging was associated with a solute depleted precipitated free zone.

6.6 On aging at higher temperatures (1073 K) or prolonged aging at 973 K, the γ'/matrix interfaces provided favourable nucleation sites for the γ'' phase giving rise to a so called "compact morphology".

6.7 A careful analysis of the experimental results has shown that certain factors control the formation and stability of the γ' and γ'' (Ni_3Nb) phases.

These factors are:

(a) The Hagel and Beattie requirements for interfacial mismatch of less than or equal to 1 pct. between precipitate and matrix is a controlling factor since the lattice mismatch between γ/γ' and γ'' was always less than 1.0 pct., when precipitation of these phases occured.

(b) The addition of iron promotes the formation of the γ'' DO_{22} phase.

(c) The calculated e/a ratios, show that the γ' phase precipitates when e/a < 8.65, while γ'' was formed when e/a > 8.65, which is in agreement with previous studies.

This is only the second known study in which the e/a ratio of the precipitating compound has been correlated with the phase stability in the same alloy.

The results strongly support that mainly the e/a ratio in addition to other less important factors is an important criterion for the prediction of γ' and γ'' formation. Therefore by proper selection of alloy chemistry and aging temperature, it is possible to control the precipitation of these phases.

Chapter VII

REFERENCES

1. D.A. Porter and K.E. Easterling, 'Phase transformations in metals and alloys', Van Nostrand Reinhold (UK) Co. Ltd., 1981.
2. 'Precipitation from solid solution', published by the American Society for Metals, Ohio, 1959.
3. J.W. Martin and R.D. Doherty, 'Stability of microstructure in Metallic systems', Cambridge press, 1976.
4. J.W. Martin, 'Micromechanisms in particle-hardened alloys', University of Cambridge press, 1980.
5. C. Wagner, Z. Electrochemi, 1965, vol. 65, p.581.
6. M. Lifshitz and V. Slyozov, J. phys. chem. solids, 1961, vol. 19, p. 35.
7. W.B. Pearson, 'Handbook of lattice spacings and structures of metals', Pergamon press, N.Y.
8. R.E. Reed-Hill, 'Physical Metallurgy principles', D. Van Norstrand Company Inc., N.Y., 1964
9. 'Metals Handbook', ASM, 8th ed., vol. 1, 1961.
10. E.C. Rollason, 'Metallurgy for Engineers', pub. E. Arnold, 1973
11. C.S. Smith, U.S. Patent , (1947).
12. M. Raghavan, Met. Trans., 1977, vol. 8A, p. 1071.

13. M. Raghavan, Met. Trans., 1978, vol. 9A, p. 734.

14. P.S. Kotval, TMS-AIME, 1968, vol. 242, p 1764.

15. I. Kirman, J. Iron steel Inst., 1969, vol. 207, p. 1612.

16. I. Kirman and D.H Warrington, Met. Trans., 1970, vol. 1, p. 2667.

17. M.C. Chaturvedi and D.W. Chung, Met. Trans., 1979, vol. 10A, p. 1579.

18. V. Ramaswamy, P.R. Swann and D.R. West, J. Less Common Met., 1971, vol. 27, p. 17.

19. O.H. Kriege and J.M. Baris, Trans. of ASM, 1969, vol. 62, p. 195.

20. D.F. Paulonis, J.M. Oblak and D.S. Duvall, Trans. of the ASM, 1969, vol. 62, p.611.

21. H.L. Eiselstein, ASTM STP 369, 1965, p.62.

22. R. Cozar and Pineau, Met. Trans., 1973, vol. 4, p. 47.

23. J.M. Oblak, D.F. Paulonis, and D.S. Duvall, Met. Trans., 1974, vol. 5, p. 143.

24. Y. Han, M.Sc Thesis, University of Manitoba, 1982.

25. W.E. Quist, R. Taggart, and D.H. Polonis, Met. Trans., 1971, vol. 2, p.825.

26. A.K. Jena and M.C. Chaturvedi, Journal of Materials science, 1984, vol. 19, p. 3121.

27. A.K. Sinha, Trans. AIME, 1969, vol. 245, p. 237.

28. A.K. Sinha, Trans. AIME, 1969, vol. 245, p. 911.

29. C. Ravindran, Ph.D. Thesis, University of Manitoba, 1982.

30. W.C. Hagel and H.J. Beattie, Trans. AIME, 1959, vol. 215, p. 967.

31. J. Helsop, Cobalt, 1964, vol. 24, p. 128.

32. A.T. Kelly and R.B. Nicholson, prog. Mat. Sc., 1963, vol. 10, p. 151.

33. M. Raghavan, Met. Trans., 1979, vol. 10A, p. 1399.

34. R. Cozar and A. Pineau, Met. Trans., 1974, vol. 5, p.2471.

35. W. Hume-Rothery, 'The Engel-Brewer Theories of Metals and alloys', Pergamon press, 1968.

36. I. Kirman and D.H. Warrington, 'Journal of the Institute of Metals', 1971, vol. 99, p. 197.

37. H.P. Klug and L.E. Alexander, 'X-ray diffraction procedures', J. Wiley and sons, N.Y, 1954, p. 726.

38. E.W. Nuffield, 'X-ray diffraction methods', J. Wiley and sons, 1966.

39. M.E. Straumanis, 'Journal of Applied physics', 1949, vol. 20, p. 727.

40. J. Nelson and P.D. Riley, Proc. Phys. Soc.(London), 1945, vol. 57, p. 160.

41. G. Cliff and G.W. Lorimer, Journal of Microscopy, 1975, vol. 103, p. 203.

42. J.I. Goldstein et. al., 'Scanning electron microscopy and x-ray microanalysis', Plenum press, NY, 1981.

43. D. Williams, 'Practical Analytical Electron Microscopy in Materials Science', Copyrighted by Philips Electronics Inst. Inc., 1984.

44. R.G. Baker, D.G. Brandon and J. Nutting, Phil. Mag., 1959, vol. 4, p. 1339.

45. F.B. Pickering, Precipitation processes in steels, Iron and Steel Institute, 1959, p. 132.

46. M. Raghavan, Met. Trans., 1980, vol. 11A, p. 993.